Volume 37, Number 1, 2011.

Mobility & Vehicle Mechanics

International Journal for Vehicle Mechanics, Engines and Transportation Systems

ISSN 1450 – 5304

UDC 621+ 629(05)=802.0

UNIVERSITY OF KRAGUJEVAC – FACULTY OF MECHANICAL ENGINEERING

SERBIAN SOCIETY OF AUTOMOTIVE ENGINEERS

M V M **M**obility **V**ehicle **M**echanics

*Editors: Prof. dr **Aleksandra Janković**; Prof. dr **Čedomir Duboka***

MVM *Editorial Board*
University of Kragujevac
Faculty of Mechanical Engineering
Sestre Janjić 6, 34000 Kragujevac, Serbia
Tel.: +381/34/335990; Tel.: 336002; Fax: + 381/34/333192

For Publisher: Prof. dr Miroslav Babić, dean, Faculty of Mechanical Engineering, Kragujevac
Ordering: Vesna Maksimović
Printed by: SaTCIP Ltd., Tržni centar Pijaca 106, 36210 Vrnjačka Banja, Serbia
tel: + 381/36/622454

Publishing of this Journal is financially supported from:
Ministry of Science and Technological Development, Belgrade, Serbia
Center of Traffic Safety, Faculty of Mechanical Engineering, Kragujevac

NOTIFICATION TO AUTHORS

The Journal MVM publishes original papers which have not been previously published in other journals. This is responsibility of the author. The authors agree that the copyright for their article is transferred to the publisher when the article is accepted for publication.

The language of the Journal is English.

Journal ***Mobility & Vehicles Mechanics*** is at the SSCI list.
All submitted manuscripts will be reviewed. Entire correspondence will be performed with the first-named author.

Authors will be notified of acceptance of their manuscripts, if their manuscripts are adopted. Authors are requested to participate in paper publishing expenses as it is described bellow:

For Native Authors: 6 pages are provided free of charge, written according to editor's given instructions. Each extra page will be charged with RSD 500 per page.
For Foreign Authors: 6 pages are provided free of charge, written according to editor's given instructions. Each extra page will be charged with €10 per page.

INSTRUCTIONS TO AUTHORS AS REGARDS THE TECHNICAL ARRANGEMENTS OF MANUSCRIPTS:

Abstract is a separate Word document, "ABSTRACT". Native authors should write the abstract in both languages (Serbian and English). The abstracts of foreign authors will be translated in Serbian for free.
This document should include the following: 1) author's name, affiliation and title, the first-named author's address and e-mail – for correspondence, 2) working title of the paper, 3) abstract containing no more then 100 words, 4) abstract containing no more than 5 key words.
The manuscript is the separate file, „TEXT" which includes appendices and figures involved within the text. At the end of the paper, a reference list and eventual acknowledgements should be given. References to published literature should be quoted in the text brackets and grouped together at the end of the paper in numerical order.

Paper size:	Max 16 pages of B5 format, excluding abstract
Text processor:	Microsoft Word
Margins:	left/right: mirror margin, inside: 2.5 cm, outside: 2 cm top: 2.5 cm, bottom: 2 cm
Font:	Times New Roman, 10 pt
Paper title:	Uppercase, bold, 11 pt
Chapter title:	Uppercase, bold, 10 pt
Subchapter title:	Lowercase, bold, 10 pt
Table and chart width:	max 125 mm
Figure and table title:	Figure _ (Table _): Times New Roman, italic 10 pt
Manuscript submission:	application should be sent to the following e-mail:

mvm@kg.ac.rs ; alex@kg.ac.rs or posted to address of the Journal:

University of Kragujevac – Faculty of Mechanical Engineering Kragujevac
International Journal M V M
Sestre Janjić 6, 34000 Kragujevac, Serbia

The Journal editorial board will send to the first-named author a free copy of the Journal offprint. Authors who are once registered in the base, will have a discount of 50% of the price for all the other issues of the Journal for the current year.

OBAVEŠTENJE AUTORIMA

Časopis MVM objavljuje orginalne radove koji nisu prethodno objavljivani u drugim časopisima, što je odgovornost autora. Za rad koji je prihvaćen za štampu, prava umnožavanja pripadaju izdavaču.

Časopis se izdaje na engleskom jeziku.

Časopis ***Mobility & Vehicles Mechanics*** se nalazi na SSCI listi.

Svi prispeli radovi se recenziraju. Sva komunikacija se obavlja sa prvim autorom.

Po dobijanju pozitivne recenzije, autor-autori participiraju u troškovima izdavanja rada i to:

Domaći autori mogu besplatno da objave do 6 strana ukupno, uređenih prema uputstvu redakcije. Za svaku daljnu stranu, autor plaća 500 dinara po strani.

Strani autori mogu besplatno da objave do 6 strana ukupno, uređenih prema uputstvu redakcije. Za svaku daljnu stranu, autor plaća 10 evra po strani.

UPUTSTVO AUTORIMA ZA TEHNIČKO SREĐIVANJE RADOVA

Rezime je poseban Word dokument, "ABSTRACT". Za domaće autore je dvojezičan (srpski i engleski). Inostranim autorima rezime se prevodi na srpski jezik besplatno.

Ovaj dokument treba da sadrži: 1) ime autora, zanimanje i zvanje, adresu prvog autora preko koje se obavlja sva potrebna korespondencija; 2) naslov rada; 3) kratak sažetak, do 100 reči, 4) do 5 ključnih reči.

Rad je poseban fajl, „TEXT" koji sadrži priloge i slike uključene u tekst. Na kraju rada nalazi se spisak literature i eventualno zahvalnost. Numeraciju korišćenih referenci treba navesti u srednjim zagradama i grupisati ih na kraju rada po rastućem redosledu.

Dužina rada:	Najviše 16 stranica B5 formata, ne uključujući rezime
Tekst procesor:	Microsoft Word
Margine:	levo/desno: mirror margine; unurašnja : 2.5; spoljna: 2 cm vrh: 2.5 cm, dno: 2 cm
Font:	Times New Roman, 10 pt
Naslov rada:	Velika slova, bold, 11 pt
Naslov poglavlja:	Velika slova, bold, 10 pt
Naslov podpoglavlja:	Mala slova, bold, 10 pt
Širina tabela,dijagrama:	max 125 mm
Nazivi slika, tabela:	Figure __ (Table _): Times New Roman, italic 10 pt
Dostavljanje rada	Elektronski

E-mail: **mvm@kg.ac.rs ; alex@kg.ac.rs** ili poštom na adresu Časopisa

Redakcija časopisa M V M
Mašinski fakultet u Kragujevcu
Sestre Janjić 6, 34000 Kragujevac, Srbija

Po objavljivanju rada, Redakcija časopisa šalje prvom autoru jedan primerak časopisa.
Autori evidentirani jednom u bazi, uživaju popust 50% za sve druge brojeve časopisa u tekućoj godini.

Mobility & **V**ehicle **M**echanics

Motorna **V**ozila i **M**otori

Volume 37
Number 1
2011.

Mobility & **V**ehicle **M**echanics

Motorna **V**ozila i **M**otori

Volume 37
Number 1
2011.

[1] PERSONALIZED VENTILATION CONCEPT IN MOBILE MACHINERY CAB

***Dragan Ružić, Ferenc Časnji**, Faculty of Technical Sciences, Novi Sad, Serbia*

UDC: 631.3:628.87

Abstract

This paper deals with an approach to air-conditioning and ventilation system design based on human thermal sensation in environment of mobile machinery cab. Taking into account specific conditions of working environment and thermal sensitivity of individual parts of human body, the idea is to obtain a microclimatic acceptable field around operator instead to make whole volume thermally uniform. Comparison of the conventional and personalized ventilation systems of the single-seat cab, by the using of the human local sensation was presented in this paper.

Key words: mobile machinery cab, thermal sensation, air distribution, ventilation, air-conditioning.

KONCEPT PERSONALIZOVANE VENTILACIJE U KABINI MOBILNE MEHANIZACIJE

UDC: 631.3:628.87

Rezime: U radu je prikazano rešenje sistema za ventilaciju i klimatizaciju bazirano na toplotnom osećaju čoveka, u okružanju kabine mobilne mehanizacije. Uzimajući u obzir specifičnosti radnih uslova i toplotne osetljivosti pojedinih delova ljudskog tela, namera je da se ostvari povoljno mikroklimatsko polje oko rukovaoca, umesto da se cela zapremina kabine učini toplotno uniformnom. U ovom radu je primenom lokalnog toplotnog osećaja čoveka izvršeno poređenje konvencionalnog sistema sa sistemom personalizovane ventilacije jednosede kabine.

Ključne reči: kabina mobilne mehanizacije, toplotni osećaj, distribucija vazduha, vemtilacija, klimatizacija.

[1] Received: September 2010. Primljen: septembar, 2010.god.
Accepted: December 2010. Prihvaćen: decembar, 2010.god.

PERSONALIZED VENTILATION CONCEPT IN MOBILE MACHINERY CAB

Dragan Ružić [1], *Ferenc Časnji*

UDC: 631.3:628.87

INTRODUCTION

We are witnesses of progressive tendency towards increased demands for comfortable environment in every aspect of human life, hence in vehicles and in work places too. Operator's seat in closed cab of work machine or tractor can be considered as both seat in the vehicle and work place. The smallest units of mobile machinery are also included in this trend, not only the larger ones. Since these machines can be powered with relatively low power engines (especially in hybrid version), extra load taken from convenient systems must be taken in account. Because the size of the cab is not proportional to the size of machine, smaller units have relatively larger extra loads, together with fact that smaller machines have lower overall efficiency compared with machines powered by larger engines. Considering this, taking the efforts to research of possibilities for reducing unnecessary energy lost is reasonable. Because operator spends most of his time at seat, it is possible to consider energy-saving strategy in this working environment [28].

Main method for reducing the energy consumption of air-conditioning (AC) is prevention of cab heating: insulation and rejection of the powertrain heat, preventing sun radiation by the size of the glasses, choice of glazing material and by the shape of the cab, to mention a few. Second method, considered in this paper, is rational use of energy by cooling first of all the operator, not the cab, bearing in mind that primary purpose of cab's AC system is to obtain thermally comfortable environment for the operator. Furthermore, in order to suite thermal environment to everyone's individual needs and obtain 100% of satisfaction, high degree of controllability is prerequisite, despite modern automatic control systems.

Personalized ventilation in the cab means that airflow characteristics are suited to human thermal sensation and that the operator has ability to adjust the system according to his personal preferences for given situation. Control of microenvironment is necessary because relationship between microclimate parameters and human thermal sensation is not reliable, due to large individual differences [23], [33]. There is also risk that AC system produce unpleasant stream of air, especially during the cool-down mode, when operator must be able to prevent this situation.

Although majority of literature about personalized ventilation and its influence on local thermal sensation and performance are related to office or laboratory chamber conditions [10], [16]-[22], [28], [30], [32], [33], the purpose of this paper is to take them as a basis for

[1] Corresponding author e-mail: ruzic@uns.ac.rs, Faculty of Technical Sciences Novi Sad, Department for Mechanization and Design Engineering, Chair for Motor vehicles, Trg Dositeja Obradovića 6, 21000 Novi Sad, tel: +381 21 485 2365

local microclimate conditions that cab's ventilation and AC system should generate around the operator. This paper is divided in following parts:

- Overview of thermal sensation and comfort models.
- Calculation of cab-operator thermal balance for typical summer conditions, taking the environment inside the cab as homogenous.
- Determination of operator's heat balance with homogenous environment as well as local heat balance for individual body parts.
- Comparison of cooling loads and characteristics between conventional and personalized approach.

At the end, main features of personalized ventilation and air-conditioning in mobile machinery cab and conclusions resulting from this example are summarized.

HUMAN THERMAL SENSATION AND THERMAL COMFORT

Humans sense the warmth or coolness of an environment through thermoreceptors located in the skin and core. The thermoreceptors sense the tissue temperatures surrounding them and send signals to the brain to interpret the environment as thermal sensation. Skin and core temperatures of the human body are regulated to release metabolic heat by convective, radiative, and evaporative heat transfer through the skin and through respiration. Main mechanisms for regulation in hot environment are change in blood flow and secretion of sweat. [7].

The human body skin surface temperature is partly determined by the rate of convective heat transfer and, hence, local air movement. Moisture on the skin has an increased effect on thermal sensation in hot conditions, particularly after sweating has been started (above PMV ≈ 0.5 [14]) [10].

Widely used Fanger's PMV (Predicted Mean Vote) model of thermal comfort is based on thermal equilibrium of human body with environment [5], [7], [13], [23]. In the model adopted in standard ISO7730, thermal comfort is scaled from -3 = cold to +3 = hot, where 0 denotes state of thermal neutrality, e.g. overall comfort, calculated from six main microclimate parameters (air temperature t_a, mean radiant temperature t_{mr}, air velocity v_a, relative humidity RH, activity M and clothing insulation I_{clo}). The model is expanded with condition that there is no local discomfort such a draught (taking the local air turbulence intensity into account) and/or thermal asymmetry. PMV index can be used in uniform environment and under steady-state conditions, within certain range of environmental parameters, making this model unsuitable for environment far from moderate (heat or cold stress). For use in environment that produces heat stress, several methods for evaluation and prediction of human thermal state are developed [23].

Parsons gives detailed analytical overview of heat exchange modes between the human's body and surroundings, from ASHRAE Handbook of fundamentals [23]. It is impossible to describe complex microenvironment such is the cab, with single point values of microclimatic parameters, therefore the models for thermal sensation based on overall thermal balance of the human body with the environment are often not appropriate. For this

reason, other so called multi-node models are developed, where human's body is presented as multi-body system consisted of core and outer layer, coupled with blood flow and regulated by thermoregulation system [4], [7], [11], [23], [31].

Models of thermal sensation depending on skin and core temperature are suitable for assessment of human thermal state based on physiological measurement, but there are not close relationships between environmental parameters and skin and core temperature. Regarding the personalized ventilation and AC, very interesting is model proposed by Hui Zhang, shortly described below [1], [2], [7], [8], [21], [23], [34]-[37].

According to Zhang's model, the body's overall thermal sensation is affected by local state of individual body parts, due to different properties and different sweating rate [1], [2], [8], [34], [37]. Individual body parts have different sensibility for warm versus cool sensations, resulting with different weighting coefficients in the model (Fig. 1):

- Back, chest, and pelvis have strong influence on overall thermal sensation, which closely corresponds to the local sensation of these parts during the local cooling.
- Hands and feet have much less influence on overall sensation, at the same rate of cooling compared with former.
- Head, arms and legs have an intermediate influence on the body's overall thermal sensation.

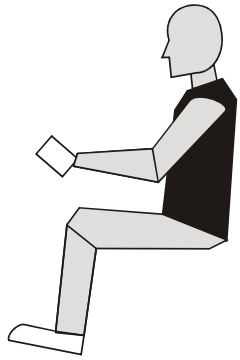

Figure 1: *Skin zones with strong (back, chest, and pelvis - black), intermediate (head, arms, legs - grey) and weak (hands, feet - white) influence on thermal sensation*

Zhang's mathematical model of thermal sensation and comfort describes the prediction of local thermal sensation as a function of skin temperature, expressed by asymmetric logistic function for static conditions [1], [34]. Sensation range was defined from -4 = very cold to +4 = very hot (extended standard 7-point scale). This local sensation prediction is based entirely on subjects' physiological data, not on environmental parameters such as the air temperatures surrounding the body. From local sensation using the regression coefficients it is possible to predict overall thermal sensation as well as local and overall comfort rating [2], [3].

During the transient conditions, the change (derivative) of skin temperature has a stronger influence on sensation than skin temperature itself, because the firing rate of

thermoreceptors is then 5 - 10 times higher [2]. Dynamic behaviour of thermal sensation in transient condition is obtained by adding of dynamic term in the equation, in analogy with Fiala's model [8]:

$$Local\ Sensation = Sensation_{static} + Sensation_{dynamic} \quad (1)$$

Influence of local airflow characteristics: velocity, temperature and turbulence

In a quiet comfortable environment, around the human body an upward free convection flow exists. Body shape and posture, air temperature, etc. define the mean velocity in the free convection flow. At comfortable room air temperature, a flow from the front of the body with a mean velocity as low as 0.1 m/s will disturb the free convection flow and above 0.2 m/s will penetrate this layer [19].

Moreover, in quiet hot environment is possible that there are complaints because absence of air movement. Perception of air movement could be taken as one of the main indicators for the overall acceptability of the conditions in ambient such is closed cab, and airflow is preferred in region of face and head. Air supply and local velocity of air must be in relation with minimum ventilation rate, while recommended values are between 10 and 20 l/s per person (36 - 72 m^3/h per person). These values are valid for buildings and cab ventilation systems generally have larger capacities, around 300 m^3/h.

There are many investigation regarding maximum permissible air velocities and turbulence intensity around human body in dependence of ambient temperature (Fig. 2) [10], [32]. Increased air speed is acceptable only if under control of operator. In general, possibility of control is more important in hot ambient.

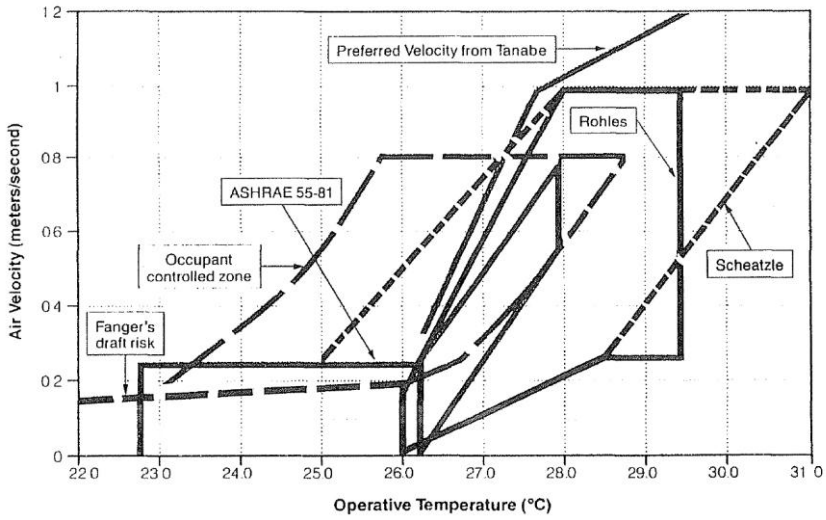

Figure 2: *Range of air velocity requirements compared among different researches, taken from [10]*

One of the most influencing parameters for thermal sensation and sensation of air quality is quality and characteristics of air in breathing zone, a semi-sphere around mouth and nose [19], [20]. From the point of perceived air quality, still air in breathing zone is not acceptable in warm ambient, even when overall comfort is achieved [3]. Cooling of breathing air has very positive results in warm environment, as opposite than heating in cold environment, regarding the influence on perceived overall comfort [2].

Airflow with higher turbulence intensity over the body part may improve operator's thermal comfort due to increased heat loss from the body, under other identical conditions in warm environments. The turbulence intensity TU is defined as the standard deviation of velocity fluctuations divided by the mean velocity. Therefore the risk of draught discomfort increases when airflow temperature decreases and mean velocity and turbulence intensity increase, and fluctuating flow may cause draught discomfort at comfortable temperatures [6], [7], [19].

The dissatisfaction about localized air stream could include dry eyes, lips and/or noses, and a cooling draft at the face and neck caused by convective heat loss [22]. Draught is defined as unwanted local cooling of the body due to air movement, and from this point of view, air velocity has more influence on local discomfort than air temperature. Therefore, possibility to control the velocity as well as the direction of the flow reduces potential negative effects of localized airflow.

According to ASHRAE standard 55-2003 and standard ISO 7730, the local discomfort can be evaluated by the index of predicted percentage of people dissatisfied due to draught (DR) in moderate environment, based on local air temperature t_a, local air velocity v_a and turbulence intensity TU [5], [7], [13]:

$$DR = (34 - t_a)(v_a - 0.05)^{0.62} \cdot (3.14 + 0.37 v_a \cdot TU)[\%] \quad (2)$$

Percentage of dissatisfied of 20% can be used as upper limit [5]. However, this model is valid for moderate conditions and cannot be extrapolated for elevated temperatures [10].

Solar radiation

Heat energy gain from the solar radiation is one of most influencing factors on thermal sensation and comfort, and one of main cause of discomfort, even in cold environment. Without any shading device, direct, diffuse and reflected radiation can create input of about 800 W/m^2, increasing the heat stress [23].

The amount of direct solar radiation energy will dependent on effective projected area. Also, the largest effective projected radiation area A_{eff} of sitting person is when azimuth and altitude angles are 30º and 15º respectively, giving the total surface equal to [7], [23]:

$$A_{eff} = A_{Du} \cdot 0.72 \cdot 0.33 = 0.238 A_{Du}\,[\%] \quad (3)$$

where $A_{Du} = 0.202\ m_b^{0.425}\ h_b^{0.725}$ is surface of human body calculated from body weight m_b and height h_b; The factor 0.72 is effective radiation area factor, and 0.33 is projected area factor [7], [23].

THERMAL BALANCE OF CAB-OPERATOR SYSTEM

Typical approach for cab cooling loads due to heat gain in hot ambient conditions (steady-state) is based on summarizing the heat gains (Fig. 3.):

1. Heat transfer through the cab envelope due to temperature difference Q_{wall}
2. Solar radiation through the glazing Q_{sun}
3. Heat released by the operator (sensible and latent) Q_H, Q_{Hw}
4. Heat from the powertrain Q_P

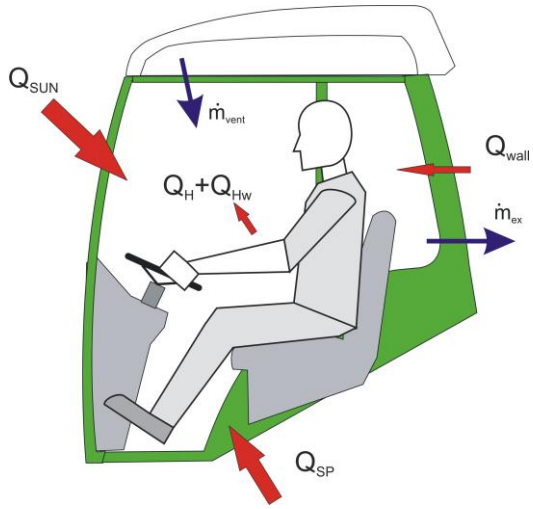

Figure 3: *Thermal balance of tractor's cab in hot environment*

The example calculation is performed for typical regional summer outdoor conditions, with outside air temperature of $t_{aout} = 30°C$, relative humidity of RH = 50%, air velocity of $v_{aout} \approx 0$ m/s and estimated solar radiation $I_{rsun} \approx 500$ W/m^2. Under assumption that environmental parameters inside the cab are uniform and steady state, interior air set temperature is $t_{ain} = 26°C$. Estimated value of mean radiant temperature is $t_{mr} = 40°C$. The inner dimensions of chosen agricultural tractor cab are 1.3 × 1.4 × 1.6 m (W × B × H), with estimated total coefficient of heat transfer through the envelope of about U = 10 W/m^{2}K [24].

The metabolic activity of the operator is chosen to be M = 1.4 Met = 1.4 · 58 W/m^2 = 81 W/m^2, and clothing insulation for typical summer working garments (t-shirt, trousers and shoes, including the seat insulation [5]) is $I_{clo} = 0.52$ Clo. For $A_{Du} = 2.0$ m^2 ($m_b = 80$ kg, $h_b = 1.8$ m), resulting with sensible heat release of $Q_H = 160$ W, plus latent heat from released water vapour of $Q_{Hw} = 150 \div 200$ W and more, depending of sweating.

Major part of the cab heat gain belongs to solar radiation and to heat from the powertrain. Solar thermal load is depending on glass size and properties (energy absorptivity, transparency and reflectivity), radiation incident angle and solar radiation spectra. Solar radiation intensity is variable and on outer surface of cabin could be between 0 and 1000 W/m^2. For the purpose of this paper, chosen value of total heat gain from powertrain is of order Q_P = 800 W and from solar radiation is approximately Q_{sun} = 500 W [14], [15], [25].

Together with heat transfer through cab walls and assuming that there is no infiltration of outside air (cab is pressurized), sum of heat gains is approximately 1.7 kW.

Heat that should be taken from intake air at the evaporator of AC is calculated for air that leaves the evaporator at 5°C. If it is assumed that air leaves the cab under the same conditions as in the (homogenous) cab interior, at 26°C, evaporator should exchange around 4 kW of heat and air mass flow should be around $\dot{m} = 250\,m^3/h$ (without recirculation, all air is passing through the air-conditioner). These values are significant considering that this capacity serves only for single person and for steady-state conditions.

Operator's thermal balance and comfort for homogenous environment

Simple method for evaluation of thermal state of the operator in cab under mentioned conditions is by using PMV index. For typical cab design with roof-mounted air-conditioning system and ceiling outlets, mean air velocity in the cab v_{ain} = 0.5 m/s was chosen according to ISO 7730 [13], as acceptable for relevant operative temperature:

$$t_o = 0.6t_a + 0.4t_{mr} = 0.6 \cdot 26 + 0.4 \cdot 40 = 31.6°C \tag{4}$$

From cooling load calculation, moisture content in cab corresponds to relative humidity of about 30%. Resulted PMV index is 1.53, which gives PPD (Predicted Percentage of Dissatisfied) of 52.8%. This means that conditions inside the cab are uncomfortable warm. However, looking at the ways of heat loads of the cab it can be noticed that direct solar radiation on the operator's body was not taken into the consideration. The equation for PMV calculation neglects direct solar load and sweating, meaning that actual thermal sensation could be different.

Using the analysis of individual heat transfer processes that occurs between the human body and environment, offers the more detailed insight in both individual and environmental factors that influence the thermal effects. Calculation of heat transfers was done for the same input data as for calculation of PMV index. Equation of heat balance is [23] (Fig. 4):

$$M = C + R + E_{sk} + C_{res} + E_{res} - R_s \tag{5}$$

Heat loss from the outer body surface (bare skin and clothes surface of clothing) is consisted of convective (C) and radiative heat loss (R), and heat loss by evaporation from the skin (E_{sk}) [7], [23]. During the respiration, heat is exchanged by dry convective heat

exchange due to difference between inhaled and exhaled air (C_{res}), and due to change in moisture content in exhaled air (E_{res}). Solar load (R_s) has a minus sign, because it can be only heat gain (or equal to zero if there is no solar radiation).

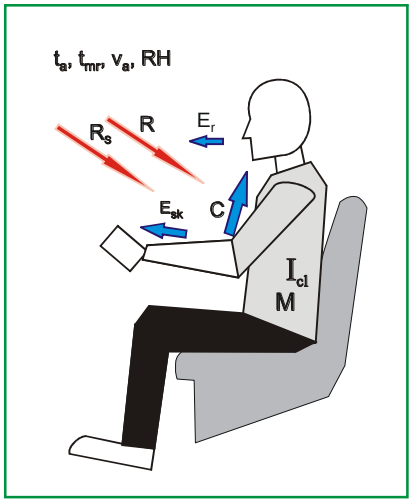

Figure 4: *Heat exchange between the operator and environment inside the cab in hot environment*

For estimated average skin and core temperatures for warm environment (slightly higher values than neutral: t_{sk} = 35°C, t_{core} = 37°C, respectively), average convective heat transfer coefficient is h_c = 5.48 W/Km^2. Temperature of the outer surface of the clothing is determined by iteration, and resulting heat loss by convection is C = 60 W.

Using the recommended method for calculation of radiative heat transfer coefficient value, heat transfer by radiation between the outer body surface and surrounding surfaces (cab interior) is R = -80 W. Minus sign denotes heat gain, as a result of higher temperatures of cab inner surfaces.

Heat loss by respiration will be equal to E_{res} + C_{res} = 15 W, determined by activity, air temperature and air humidity.

In order to maintain body heat balance, coefficient of wettedness is calculated from resulting difference between total heat gain and required heat loss from the skin by evaporation, as the only way for natural "cooling" of the body in warm and hot environment. Through the evaporation of the sweat is necessary to remove 167 W of excessive heat. Clothing ventilation effects are not taken in consideration, mainly due to insufficient data and due to fact that operator is more or less still in the machinery seat.

If there is no direct solar load on operator, coefficient of skin wettedness would be w = 0.41. Recommended value for comfort for M = 1.4 Met would be almost at minimum, e.g. w = 0.07 (ratio of required heat loss by evaporation and maximum heat loss by evaporation

[23]). Assuming the solar load of R_s = 100 W (determined from direct solar load on cab outer surface I_{rsun} = 500 W/m^2, single-layer tinted glass total energy transmittance and area of operator's body surface exposed to the solar radiation through the cab glazing), required coefficient of wettedness rises to w = 0.66. This corresponds to sweating rate of 0.51 kg/h, taking into account the sweating efficiency [23].

This example is valid for homogenous environment, as mentioned before. Actually, main non-homogeneity belongs to the air velocity distribution and radiant asymmetry. Next part of the paper will deal with human-based approach for the generating of comfortable microenvironment in the cab of mobile machinery.

BASIC PRINCIPLES OF PERSONALIZED VENTILATION IN CAB

Personalized ventilation is based on the principle that every part of the body has to have heat exchange with the environment which is suited with current thermal demand, in order to achieve or keep local and overall thermal sensation within the values that in combination produce state of thermal comfort.

The personalized ventilation and AC system is defined by local airflow temperature and mean velocity, turbulence intensity, direction and distance of outlet from the body part. Based on numerous researches with human subjects exposed to the personalized ventilation under the various conditions, the main features of personalized ventilation in the cab are given below [2], [16], [17], [18], [19].

Temperature of localized air should be equal or 3÷4ºC lower than the interior air temperature. Airflow local velocity should have the ability to penetrate the operator's free convection flow, and as a minimum target velocity can be taken velocity of 0.3 m/s. The individually preferred maximum velocity can be as high as 1.5 m/s, especially at interior air temperatures above 26ºC.

The system should generate localized flow with a uniform velocity profile and low initial turbulence, therefore outlets with large circular cross-section are recommended. Air supply at low turbulence intensity maintains higher speed along the flow path, minimizing the mixing with surrounding air. This also enables easier control of parameters of air jet impinging the body surface. A circular outlet will generate a jet with a much longer potential core region than a rectangular outlet with the same cross-section area.

The location of outlets should enable use of the initial region of the personalized flow (3 to 6 outlet diameters), and this can be achieved on distances from 0.4 to 0.6 m from the operator. This must be in agreement with the geometry of interior space of the cab. Ventilation nozzles should also be placed in such a way to supply air from the side into the operator’s breathing zone, in order to avoid dry-eye and draft discomfort (typical for air impinging on the back of the neck). Airflow from the front against the face is also preferable.

System should enable wide range of control of velocity (flow rate) and direction of the personalized flow, as well as the air temperature. It is easier to control and change velocity

and direction of airflow than air temperature. For example, when the operator is warm and wants rapid cooling, he points the airflow directly at him. Under average conditions, operator will not tolerate a strong jet of air in the face for a substantial length of time, but he will prefer to feel only a light air movement on his face together with good circulation of the air within the cab.

Thermal balance of the operator's body parts exposed to the localized airflow

If the heat generation within the body is weighted according to volume of individual body parts, dividing the body onto the head, trunk, arms and legs, for the same data as in previous example, using the neutral skin temperatures, heat loss from individual parts is presented in Table 1. This was done for three air jet temperatures: 24, 25 and 26°C. (Lower air temperatures result with lower temperature of clothing surface, therefore heat exchange by radiation slightly increases.)

Table 1: *Body parts volumes, surfaces and heat generation (according to Stolwijk and Hardy 25-node model [23]) Hands and feet are incorporated into the arms and legs respectively, due to simplification. Arm and leg skin temperatures are averaged for upper and lower parts of limbs.*

Segment	Surface area, m^2	Volume, $m^3 \cdot 10^{-3}$	Heat load for air jet temperatures of 24, 25 and 26°C ($M+R+R_{sun}$), W			Skin temperature (neutral), °C [34]
Head	0.14	4.32	19	19	19	35.5
Trunk	0.72	44.09	194	192	190	35.4
Arms	0.37	8.31	37	36	36	34.4
Legs	0.77	23.28	103	102	101	33.4
Total	1.99	80.00	353	349	346	-

In this approach, heat flow within the body caused by blood flow is not taken into consideration. This could be corrected by using the some of valid mathematical models of human thermoregulation system.

In order to cool body parts, e.g. to maintain neutral skin temperature, air jet should be such that convective heat transfer is sufficient to remove the heat with minimum sweating. Head, hands, arms and sometimes lower legs are not covered with clothes in summer period, consequently are directly exposed to convective heat transfer and the reaction is fastest in transient conditions. General methods for calculating the convective heat transfer coefficient are applied, using the values from Table 1 and treating the arms as cylinders and the head as a sphere, under assumption that air velocity is uniform along the arm and perpendicular to it [12]. Under conditions of thermal equilibrium between heat generation within the body parts and convective heat loss, maintaining the basic requirement for preventing the discomfort, local air temperatures and velocities are given in Table 2, for arms and head.

Table 2: *Relationship between required air velocities and given local air temperatures for thermal equilibrium of the arms and the head*

Segment	Local air temperature $t_{a\ local}$, °C	Air velocity, $v_{a\ local}$, m/s
Head	24	0.13
	25	0.15
	26	0.18
Arms	24	0.78
	25	0.93
	26	1.12

Calculated convective heat transfer coefficients are in range of 3.3 - 3.9 W/m^{2}K for head and 9.6 - 11.6 W/m^{2}K for arm. Values for the head are in good agreement with values given by Stolwijk and Hardy in [23]. Maximum draught rate in the head zone for highest air velocity (0.18 m/s), calculated according to eq. 2 is in range of 9 ÷17.5% < 20%, for TU = 10 ÷ 70%.

In the case of arm, calculated coefficients are higher than the value from the same source, indicating that heat generation within the arms is probably overestimated. Required local air velocities are also too high for air jet temperatures (Figure 1.). Also the coefficients of convective heat transfer are given for cylinder in cross flow, but due to actual jet spreading and position of the arms, streamlines would not be perpendicular to the arm, making these results suitable for comparison purposes only.

Trunk and legs are covered with clothing, and heat transfer mechanisms are more complex due to clothing heat and vapour insulation, ventilation through the clothing layers and differences in surface characteristics regarding convective and radiative heat transfer.

Implementation of model of the human physiological response, as mentioned, or experimental measurement on human subjects or with thermal manikin under the same conditions will give more realistic resulting heat distribution over the body, local skin temperatures and air velocities.

Cab cooling load in the case of non-homogenous environment

From theoretical approach for cooling load calculation, heat that has to be removed from intake air at the evaporator is proportional to the cab heat gain (solar load and heat from powertrain are prevailing here) and to the difference between enthalpy of outside air and enthalpy of air that leaves the cab. In the example with homogenous environment inside the cab, it was assumed that air was leaving the cab at temperature of 26°C. In the case where principle of personalized ventilation is used, resulting air temperature at the exhaust opening would be certainly higher, because there is no need to cool entire volume of air in the cab, but only operator's body. For example, if the air at the exhaust has the temperature of 28°C or even 30°C instead of 26°C, estimated cooling load at the evaporator would be theoretically lower by about 15% or 30%, respectively. Of course, this is theoretical approach for comparison purposes, with many parameters being neglected and many others

empirically estimated or rounded, thus generating the cumulative errors.

For proper evaluation of the system thermal behaviour and obtaining actual and realistic values for chosen cab design, it is necessary to model complete cab-operator-environment-HVAC system. The modelling process should include exact thermal properties of cab envelope, solar and powertrain thermal loads, airflow field analysis for chosen distribution of ventilation outlets and discharge characteristics for every outlet. As the number of the outlets can be at least 6 (to independently control the conditions of head, trunk, arms and legs), it is obvious that flow field will be very complex and asymmetric. This problem could be analysed and optimised using the CFD techniques.

CONCLUSIONS

In this paper comparison between two different approach regarding thermal processes that could be encountered in mobile machinery cab during the summer period was presented. Focus was not on exact values of parameters but rather on different mechanisms of thermal interaction between the human body and the cab, because the system should have to be adaptive to personal thermal demands under the various conditions. The results of simplified theoretical calculations showed that there are energy savings potentials in favour of personalized ventilation and air-conditioning system, whose operation is based on specific mechanisms of heat transfer between individual body parts and surrounding.

The personalized ventilation should be designed in such a way that there is optimum heat loss from individual body parts for maintenance of required skin temperature, but without local discomfort, especially without draught and eye irritation in the face region, where breathing zone have to be provided with fresh and clean cool air.

Further researches in this field should include:

- Implementation of human thermal and physiological model in cab-operator-environment-HVAC system
- CFD analysis of air flow field in the cab interior for different outlet layouts and types
- Transient conditions (cool-down regime)
- Experimental validation of mathematical models with measurement of physical parameters, as well as with human subjects

One very important benefit in the use of personalized ventilation is the improvement of operator's' health, comfort and consequently working performance, where the advantages and savings due to improvement of these factors may be much higher than the savings in energy consumption of cab air-conditioning.

ACKNOWLEDGMENTS

This research was done as a part of project TR20078 "Energetic and ecological efficiency of tractors and mobile machinery", supported by Serbian Ministry of Science and Technological Development.

REFERENCES

[1] Arens E., Zhang H., Huizenga C.: "Partial- and whole-body thermal sensation and comfort. Part I: uniform environmental conditions", Journal of Thermal Biology 31, 2006, pp. 53 – 59

[2] Arens E., Zhang H., Huizenga C.: "Partial- and whole-body thermal sensation and comfort. Part II: non-uniform environmental conditions", Journal of Thermal Biology 31, 2006, pp. 60 – 66

[3] Arens E., Zhang H., Kim D. E., Buchberger Elena, Bauman F., Huizenga C., Higuchi H.: Impact of a task-ambient ventilation system on perceived air quality, Indoor Air 2008, August 17-22, Copenhagen, Denmark

[4] ASHRAE Fundamentals Handbook, Atlanta, USA, 1997

[5] ASHRAE Standard 55P. Thermal environmental conditions for occupancy, Third public review, ASHRAE Inc., 2003

[6] Fanger P. O.: "Human requirements in future air-conditioned environments", International Journal of Refrigeration 24, 2001, pp. 148-153

[7] Fanger P. O.: "Thermal comfort", McGraw-Hill, New York, 1970

[8] Fiala D.: "Dynamic Simulation of Human Heat Transfer and Thermal Comfort", PhD thesis, De Montfort University, 1998

[9] Fiala D., Lomas K., Stohrer M.: "A model of human thermoregulation: the passive system", Journal of Applied Physiology, 87, 1999, pp. 1957-1972,

[10] Fountain M., Arens E., de Dear R., Bauman F., Miura K.: "Locally Controlled Air Movement Preferred in Warm Isothermal Environments", ASHRAE Transactions, 1994, Vol. 100, part 2

[11] Gagge A. P., Stolwijk J. A. J., Nishni Y.: "An effective temperature scale based on a simple model of human physiological regulatory response", ASHRAE TRANSACTION, Vol. 77, Part I, 1970, pp. 247-260

[12] Incropera F. P., DeWitt D. P.: Fundamentals of heat and mass transfer, John Wiley & Sons, USA, 1981

[13] ISO 7730. Moderate thermal environment- Determination of the PMV and PPD indices and specification of the conditions for thermal comfort. International Organization for Standardization, 1994

[14] Jahns G. von, Janssen J.: Klimatizierung von Fahrerkabinen landwirtschaftlicher Fahrzeuge, Grundl. Landtechnik Bd 32, 1982, pp. 164-171

[15] Janssen J.: Luftführung in Fahrerkabinen unter dem Gesichtspunkt der thermischen Behaglichkeit, Grundl. Landtechnik 34, Nr 5, 1984, pp. 198-205

[16] Kaczmarczyk J., Melikov A., Silva D.: "Effect of warm air supplied facially on occupants' comfort", Building and Environment 45, 2010, pp. 848–855

[17] Khalifa H. E., Janos M. I., Dannenhoffer J. F.: "Experimental investigation of reduced-mixing personal ventilation jets", Building and Environment 44, 2009, pp. 1551–1558

[18] Liu C., Higuchi H., Arens E., Zhang H.: "Control of the Microclimate around the Head with Opposing Jet Local Ventilation", Healthy Buildings, 2009, September 13-17, Syracuse, NY

[19] Melikov A.: "Personalized ventilation", Indoor Air 2004, 14 (Suppl. 7): pp. 157–167

[20] Melikov A., Cermak R., Majer M.: "Personalized ventilation: evaluation of different air terminal devices", Energy and Buildings 34, 2002, pp. 829–836

[21] Nan G.: "Human perception of local air movement in the tropics", PhD thesis, National University Of Singapore, 2005

[22] Niu J., Gao N., Phoebe M., Huigang Z.: "Experimental study on a chair-based personalized ventilation system", Building and Environment 42, 2007, pp. 913–925

[23] Parsons K.: "Human thermal environments: The effects of hot, moderate and cold environments on human health, comfort and performance", 2nd ed. Taylor & Francis, London, 2003

[24] Rugh J., Farrington R.: Vehicle Ancillary Load Reduction Project Close-Out Report, Technical Report NREL/TP-540-42454, 2008

[25] Ružić D., Časnji F., Muzikravić V.: Glass properties as an influencing factor on microclimate in tractor cab (in Serbian), Tractors and power machines, Vol. 12, No. 4, 2007, pp. 92-97

[26] Ružić D., Časnji F., Muzikravić V.: Thermal load on passengers in an automobile cabin, in proceedings of International Congress Motor Vehicles & Motors 2006, Kragujevac, 2006

[27] SAE J1503, Performance test for air-conditioned, heated and ventilated off-road self-propelled work machines, 1986

[28] Schiavon S., Melikov A. K.: "Energy-saving strategies with personalized ventilation in cold climates", Energy and Buildings 41, 2009, pp. 543-550

[29] Spentzas C., Demić M.: Development perspectives of vehicle's automotive systems, Mobility and Vehicle Mechanics, Vol 28, Number 1-2, 2002.

[30] Sun W., Tham K. W., Zhou W., Gong N.: "Thermal performance of a personalized ventilation air terminal device at two different turbulence intensities", Building and Environment 42, 2007, pp. 3974–3983

[31] Tanabe S.-i., Kobayashi K., Nakano J., Ozeki Y., Konishi M.: "Evaluation of thermal comfort using combined multi-node thermoregulation (65MN) and radiation models and computational fluid dynamics (CFD), Energy and Buildings 34, 2002, pp. 637-646

[32] Toftum J.: "Air movement – good or bad?", Indoor Air 2004; 14 (Suppl 7), pp. 40–45

[33] Watanabe S., Melikov A. K., Knudsen G. L.: "Design of an individually controlled system for an optimal thermal microenvironment", Building and Environment 45, 2010, pp. 549-558

[34] Zhang H.: "Human Thermal Sensation and Comfort in Transient and Non-Uniform Thermal Environments", PhD thesis, University of California, Berkeley, 2003

[35] Zhang H., Arens E. A., Huizenga C., Han T.: "Thermal sensation and comfort models for non-uniform and transient environments: Part I: local sensation of individual body parts", Building and Environment 45, 2010, pp. 380–388

[36] Zhang H., Arens E. A., Huizenga C., Han T.: "Thermal sensation and comfort models for non-uniform and transient environments: Part II: local comfort of individual body parts", Building and Environment 45, 2010, pp. 389–398

[37] Zhang H., Arens E. A., Huizenga C., Han T.: "Thermal sensation and comfort models for non-uniform and transient environments: Part III: whole-body sensation and comfort", Building and Environment 45, 2010, pp. 399-410

[1] VEHICLE IN-USE EMISSIONS TESTING AND PORTABLE EMISSIONS MEASUREMENT SYSTEMS (PEMS)

Velimir Petrović, Branka Grozdanić, Đuro Borak, *IMR Institut, Belgrade, Serbia*

UDC: 621.43.068

Abstract

The growing concern in Europe about health effects caused by pollution levels has led to an intensification of the related research. In this context, Portable Emissions Measurement Systems, or PEMS measure emissions from combustion engines as the vehicle is being used. This technology allows real-world in-service testing and provides more data than the conventional laboratory engine or vehicle test cells. PEMS offer a modern and innovative counterpart to check the impact of emissions from combustion engines upon the environment. PEMS provide a complete and very accurate real-time monitoring of the gaseous pollutants emitted by the engines (HC, CO, CO2, NOx). However, the testing of particle emission is bigger problem because still there is not available measurement system.

This paper presents the European PEMS program, aiming at checking the feasibility of PEMS instruments to measure accurately particle mass at low PM emission levels of road and non-road vehicles. Several portable commercial instruments, using different principle of operation (Dekati DMM and EtaPs, Horiba TR-OBM, Sensors PPMD, AVL Micro Soot Sensor, Control System micro-PSS) are included in the program as candidate instrument. The principles of operation of these instruments are explained in the paper.

Key words: exhaust emission, diesel engine, particles, measurement, PEMS.

ISPITIVANJE EMISIJE VOZILA U EKSPLOATACIJI I PRENOSIVI SISTEMI ZA MERENJE EMISIJE (PEMS)

UDC: 621.43.068

Rezime: U Evropi raste zabrinutost u vezi štetnih dejstava izazvanih visokim nivom zagađenja što je dovelo je do intezivnijeg istraživanja na ovom polju. Pri tome posebnu pažnju privlače Prenosivi Sistemi za Merenje Emisije ili skraćeno PEMS za merenje emisije moroa SUS dok je vozilo u normalnoj eksploataciji. Ova tehnologija omogućava ispitivanje emisije motora SUS u stvarnim radnim uslovima eksploatacije, i pri tome pruža više podataka nego konvencionalno laboratorisko ispitivanje motora ili vozila u probnoj stanci. Stoga PEMS nudi moderne i inovativne konkurente postojećim uređajima za proveru uticaja izduvne emisije iz motora unutrašnjeng sagorevanja na čovekovu okolinu. PEMS obezbeđuje kompletan i vrlo precizan trenutni monitoring gasnih zagađivača

[1] Received: September 2010. Primljen: septembar, 2010.god.
Accepted: December 2010. Prihvaćen: decembar, 2010.god.

emitovanih od strane motora (HC, CO, CO2, NOx). Međutim, ispitivanje emisije čestica je znatno veći problem jer za sada ne postoji komercijalno raspoloživi merni sistem.

Ovaj rad prikazuje PEMS program Evropske Unije, koji ima za cilj da ispita pogodnost prenosivih instrumenata za precizno merenje niske emisije čestica vozila sa dizel motorima. Nekoliko komercijalno dostupnih prenosnih instrumenata, koji koriste različite principe rada (Dekati DMM and EtaPs, Horiba TR-OBM, Sensors PPMD, AVL Micro Soot Sensor, Control System micro-PSS) su uključeni u ovaj program kao potencijalni budući standardni uređaj. Princip rada ovih instrumenata je objašnjen u ovom radu.

Ključne reči: izduvna emisija, dizel motor, čestice, merenje, PEMS.

VEHICLE IN-USE EMISSIONS TESTING AND PORTABLE EMISSIONS MEASUREMENT SYSTEMS (PEMS)

Velimir Petrović [1], Branka Grozdanić, Đuro Borak

UDC: 621.43.068

INTRODUCTION

Why Portable Emissions Measurement Systems (PEMS)? New tehnologies for extra low engine emissions put new question: does emission testing in standard laboratory corresponds to real life emission of vehicle in-use? To answer this question it is necessary to measure vehicle in-use emission. However, such testing is very complex and still there is not reliable and appropriate portable emission measurement system which can be used in real -service vehicle operation.

PEMS represent a robust and accurate solution to study the in-use emissions of combustion engines and are becoming part of the emissions control regulations, as evidenced by the latest requirements introduced in the United States. The European Union is currently following the same route to check the in-use behavior of heavy-duty diesel vehicles. The European Commission launched in January 2004 a co-operative research program (the EU-PEMS Project) involving the European heavy-duty engine manufacturers and PEMS suppliers. The PEMS Pilot Program shall facilitate the introduction into the European heavy-duty vehicle emissions legislation the use of PEMS as a tool for in-service conformity (ISC). The application of PEMS is ranging from large heavy duty engines to the smallest light-duty vehicles and more recently to off-road mobile machinery. The current commercially available PEMS for gaseous exhaust measurements exhibit measurement performances that are close to the ones of laboratory grade systems. While instrumentation and the test methods are mature for gaseous emissions, the development of portable PM instruments and their test protocols remain a complex challenge, as simultaneous progress takes place in engine and after-treatment technologies. EU PEMS program has to solve all these problems and the aim of this review is to present this program based on the work carried out at European Commission – DG Joint Research Centre, Institute for Environment and Sustainability - Transport and Air Quality Unit in Ispra, Italy [1].

Currently, only two PEMS are commercially available to measure the gaseous regulated emissions (THC, CO, NOx + CO2). Both systems are compliant with the only official standard the US CFR Part 1065 [5]. To measure PM emissions on-board several technologies and instruments are currently available and more effort is ongoing to make these technologies more compact and suitable for on vehicle testing. The instruments, to be eligible for the measurement program, had to meet the following criteria:

- be traceable (or at least present some correlation) to the heavy-duty laboratory standard instruments in terms of dilution and total PM mass measurements;

[1] Corresponding author e-mail: imr-institut@eunet.rs, IMR Institute,Patrijarha Dimitrija 7-13, 11090 Belgrade, Serbia

- provide “real-time” (second-by-second) information on the total PM concentration in the diluted or raw exhaust of the vehicle;
- be commercially available or at least advanced prototypes that are close to a commercial application.

As one of the main criterions for the portable PM instrumentation is its traceability to laboratory standards. Several aspects of the standards have been considered such as the sensitivity for future low PM levels, the sampling and dilution techniques and the mass measurements method. Great effort has been undertaken to improve the detection limit, above all for modern low-emission engines. This resulted in Environmental Protection Agency (EPA) 2007 regulation [2] where new filter media, higher resolution of the balance, tighter tolerances for the temperature and so on allow lowering the detection limit. A pre-classifier (cyclone) is also used to prevent the coarse material to be deposited on the filter.

A similar approach has been proposed for future European regulations, which has been extensively tested and compared to the existing method with new guidelines proposed for PM and particle number within the PMP program [3]. However, a great doubt that remains is whether artifact free measurements are possible. Furthermore, the new ISO 16183 standard [4] specifies the measurement and evaluation methods for gaseous and particulate exhaust emissions from HDVs under transient conditions on a test bed. It focuses on the introduction of Partial Flow Sampling Systems (PFSS) and the procedure defined can be applied to any transient test cycle that does not require extreme system response times. In PFSS, a small, but proportional to the total flow, fraction of the total exhaust is sampled and used for the determination of the PM emission rate. The proportionality ratio between sampling flow and total exhaust flow is often called “split ratio” and needs to be kept constant throughout the measurement. Also it has to be seen how to pass from laboratory standards to on-board PM measurements.

THE OBJECTIVE EU PEMS PROGRAM

The main objectives and the scope of the EU PEMS program are:

- To validate the use of PEMS for in-service conformity (ISC) of heavy-duty engines;
- To evaluate the PEMS test protocol and its implementation by the participants;
- To provide further information on incorporating the PEMS approach in the European type-approval legislation;
- To develop and share 'best practice' approach for the use of PEMS in ISC testing to all relevant stakeholders;
- To benchmark the dialogue between manufacturers and type-approval bodies;
- To address open technical issues of the PEMS Project (in particular use of after-treatment systems, cold start and PM measurement).

The current work has to evaluate the measurement performance of the candidate portable systems compared to a standard method and also to check their sensitivity for the future low PM emissions standards. However, the criteria must be fulfilled to use the systems on road

and maybe non-road vehicles. The on board application of the standard PM measurement principles is challenging as PEMS are required:

- to be small, lightweight and easy to install;
- to be simple to operate;
- to work with low power consumption,
- to have good sensitivity for low PM concentrations
- to have a low to medium cost.

Additionally, the portable candidate systems have at least to:

- sample and dilute the vehicle exhaust according to existing standards (ISO16183, US standards);
- provide the total PM mass over a test cycle, by collecting the PM on a media and/or integrating data ;
- provide test data compatible with the work/CO2 averaging window method and/or the US-NTE standards.

Also, the portable candidate systems have to face two challenges:

- the installation on the vehicles: how shall the equipment be installed and the exhaust sampled and conditioned;
- the post-test evaluation method.

The first point above is delicate in the sense that the portable instrument shall be as compact as possible. When measuring gaseous emissions, the exhaust gas is sampled from the tailpipe and taken to the gas analyzers using a heated sampling line. The length of the line (3 or 5 meters) offers the flexibility to install the PEMS in the cabin or on the load area of a truck. When measuring PM emissions, the use of a (long) sampling line is critical as losses may occur by deposition on the line and therefore affect the total PM collected by the instrument. The best way to minimize losses is to install the PEMS PM as close as possible to the sampling point, i.e. close to the tailpipe of the vehicle. Unfortunately, the layout of the exhaust system on European trucks does not allow to place near the tailpipe any device whose size would be close to the one of a gaseous PEMS. To overcome the problem, it was proposed in this program:

- to accept the losses caused by the transport of the diluted or raw exhaust:
- to freeze the geometry of the sampling/transport line to 5 meters;
- to allow for the transport of the raw or the diluted exhaust, depending on the engineering strategy followed by each instrument manufacturer.

Another objective of the program is to understand how the measurement techniques proposed to estimate the PM mass accumulation rate compare to each other. It is also envisaged to determine which candidate instruments and technologies are the most suitable and if they will be sensitive enough, especially at low emission levels.

At the same time, the experiences with instruments for particle number measurement, gained during PMP program, are welcome. A variety of aerosol instrumentation is available for particle number and size measurements [5]: TSI Scanning Mobility Particle Sizer (SMPS), Condensation Particle Counter (CPC), Dekati Electrical Low Pressure Impactor (ELPI), TSI Engine Exhaust Particle Sizer (EEPS) and Cambustion Differential Mobility Spectrometer (DMS). The Diffusion Charger (DC) can be used to measure particle surface area, which is converted to mass concentration [5].

CANDIDATE INSTRUMENTS

The principle of operation of interesting candidate instruments will be discussed shortly.

A picture of the portable Control Systems m-PSS is shown in Figure 1. This is a prototype portable instrument working according the PFS principle; it uses a 47 mm filter and collects PM with a filter face velocity of 43 cm/s at a filter temperature of 44 ± 1ºC. In its standard laboratory configuration (PSS-20), it uses filters of same type but with 70 mm diameter of as for the PTS method [6].

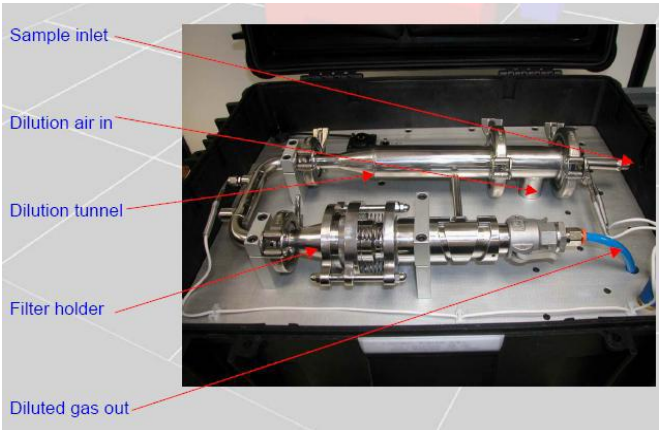

Figure 1: *Control Systems m-PSS*

The AVL Micro Soot Sensor (MSS), based on photo-acoustic measurement principles [7] was used as it is possible to do transient measurement of soot concentration with high sensitivity (detection limit ≤ 10 μg/m³: ~5 μg/m³). Its working principle is shown in Figure 2. The exhaust gas is directed through a measuring chamber and thermally animated by a modulated laser beam; modulated heating produces periodic pressure pulsation, which will be detected by a microphone as acoustic wave. The signal is then amplified in a pre-amplifier and filtered in a „Lock-In"- amplifier. The MSS was used to measure exhausts directly at the tailpipe by using its own exhaust conditioning unit with a dilution ratio of 10; the latter allows a dilution with constant ratio up to 10 (partial dilution) and a conditioning of the diluted exhaust (temperature below 60ºC and pressure at ambient ±50 mbar). No correction for losses or additional MSS calibration was needed when using its exhaust conditioning unit.

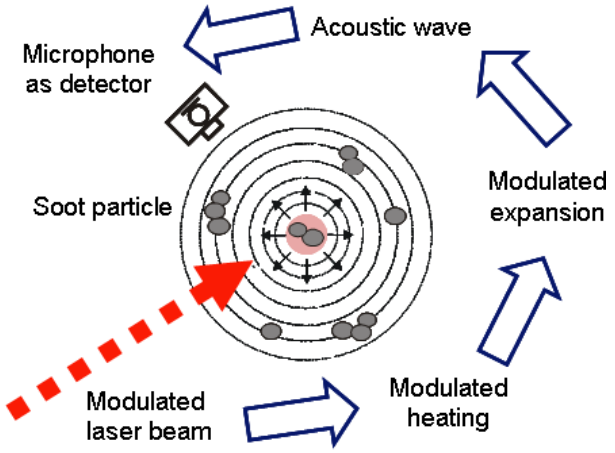

Figure 2: *AVL Micro Soot Sensor*

Based on the well-known ELPI™ technology, the Dekiati DMM 230 (Figure 3) consists of a corona charger complete with on-line particle density measurement, and an inertial 6-stage impactor with electrical detection [8]. A diffusion charger is used to give precisely determined charge to all measured particles. Charge level is close to saturation charge level for each particle size. After the charging region a static electrical field is used to deflect smallest particles to the charger mobility electrode; an electrometer is used to measure this current. This construction is used as a particle mobility size analyzer. After the charger particle size classification is accomplished in a 6-stage inertial impactor. Sensitive electrometers are connected to impactor collection sensors and particles impacting to a corresponding collection plate generate an electrical current for that electrometer. This current is proportional to the amount of particles in each size range. Combining the particle mobility size information from the charger and aerodynamic size from the impactor enables calculation of the effective density of the particles required for conversion from measured current values to particle mass concentration.

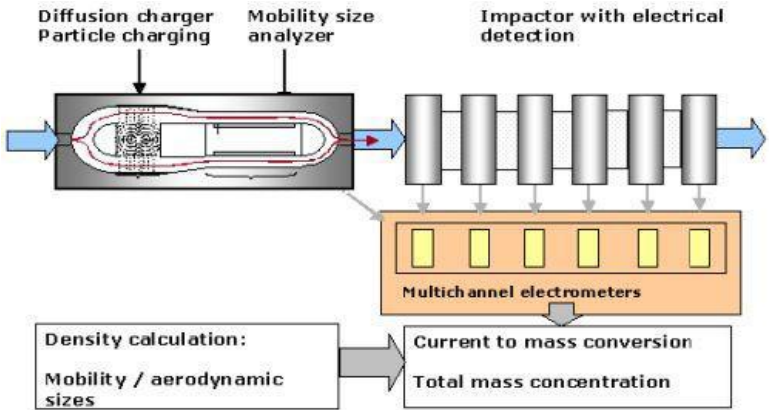

Figure 3: *Dekati DMM*

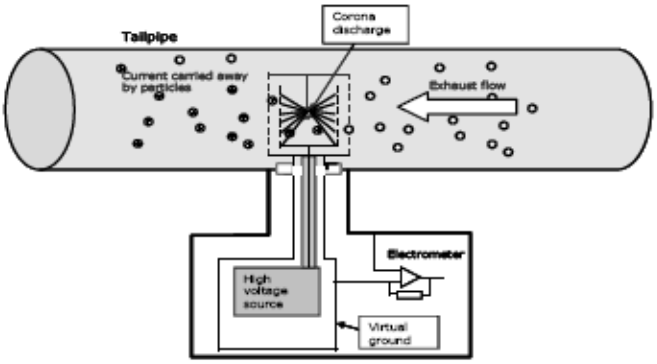

Figure 4: *Dekati ETaPS*

The Electrical Tailpipe PM Sensor (ETaPS), based on electrostatic principles for particle detection in real time has been introduced also by Dekati [9]; this is a new-sensor type device for in-situ tailpipe PM measurements. When exhaust flow passes through the inner charging chamber a known amount of charge is attached to all solid and volatile particles. The charge carried by particles leaving the outer charging cage is then measured with a sensitive electrometer. This signal is proportional to the amount of particles emitted by the engine. Figure 4 shows its working principle.

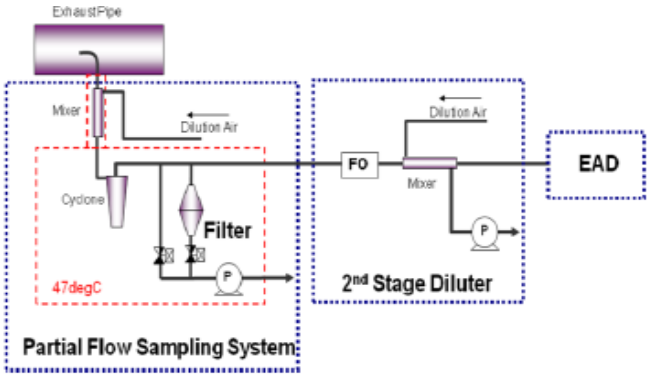

Figure 5: *Horiba OBS-TRPM*

The Horiba OBS-TRPM is a filter based partial flow diluter, provided with a cyclone (cut point at 6 um) and PM sampling at 47 C. In addition, it is provided with a diffusion charge sensor (DCS) that is sued as PM detector and it measures the particle length in real time, with the assumption that the mass accumulated on the filter is proportional to the PM length parameter [10]. The OBS-TRPM will typically last about 8 hours for a trap equipped vehicle with moderate NTE operation. The probe should be installed so that it is facing upstream in the center of the exhaust flow (+/- 1/10 of the pipe diameter). The partial flow sampling system will extract a proportional amount of raw exhaust and dilute with HEPA filtered dilution air (through PZ-1 and CFO-1). The total flow through the heated transfer line is then 30 lpm. A small amount of this diluted exhaust is bypassed to the DCS module

for real time measurement. This flow is measured by an orifice in the DS module. The rest of the diluted exhaust is either passed through the analytical filter or goes through a bypass filter. Dilution gas is added through MFC-2 to make up for the diluted exhaust bypassed to the DC unit. The total diluted exhaust is measured at the VFM2 at 30 lpm. The makeup of MFC1 is used to maintain the 30 lpm flow even when the total pump flow varies. This system will now give a transient response (DCS) correlating to a PM mass collected on a filter.

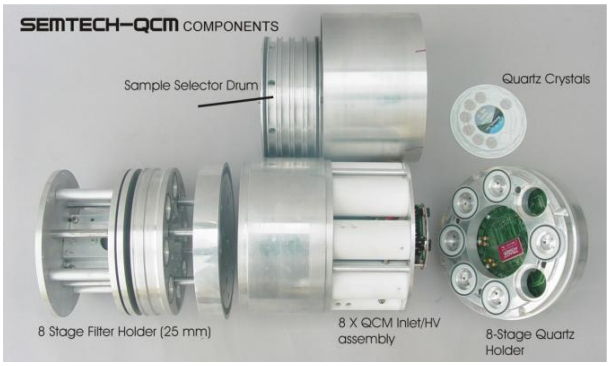

Figure 6: *Sensors SEMTECH PPMD*

The portable particulate mass measuring device (PPMD) by Sensors is based on the Quartz Cristal Microbalance (QCM) technique for PM mass measurements (Figure 6). It is composed of two micro-proportional sampling systems (MPS) for exhaust dilution and a carousel quartz crystal microbalance (CQCM) consisting of eight quartz crystals [11]. The second MPS is to allow for additional dilution. The initial dilution is at the downstream end of the sample inlet capillary (for capillary flow control). The second is at the upstream end of a venturi throat (downstream of the transport capillary containing the sample and primary dilution). This secondary dilution creates a pull or suction on the end of the second or transport capillary. The sample capillary flow control dilution (or primary dilution) is at a pressure higher than the venturi (secondary) dilution point (i.e., $P2 > 0$). The constraints for this diluter are the total flow through the sampler, i.e., sample flow plus primary dilution flow plus secondary dilution flow, is held constant and the sample flow is controlled to always be proportional to the exhaust flow.

CONCLUSIONS

This paper work gives some insights into the European PEMS PM evaluation program still ongoing at the Joint Research Centre (JRC). Several portable commercial instruments, using different principles of operation, gravimetric and non gravimetric methods, have been considered as candidate instruments for the program. These are:

- Control Sistem m-PSS
- AVL Micro Soot Sensors (MSS)
- DEKATI DMM

- DEKATI ETaPS
- Horiba OBS TRPM
- Sensors SEMTECH PPMD

The EU PM PEMS project is currently evaluating all candidate instruments and should suggest the best solution and test protocol for vehicle in-use emission testing.

ACKNOWLEDGMENT

Special thanks to Institute for Environment and Sustainability (IES) at JRC, Ispra, for the opportunity to introduce me with EU PEMS program, as well as to all colleagues in the Vehicle Emission Laboratory (VELA 5) at JRC, ISPRA, for friendly cooperation.

REFERENCES

[1] Rubino L., Bonnel P., Carriero M., Krasenbrink A., "Portable Emission Measurement System (PEMS) For Heavy Duty Diesel Vehicle PM Measurement: The European PM PEMS Program", SAE Technical Paper 09ICE-0015, 2009.

[2] -US Environmental Protection Agency. (2001). Control of air pollution from new motor vehicles: heavy duty engine and vehicle standards and highway diesel fuel sulphur control requirements; Final Rule. 40 CFR Parts 69, 80, 86. Federal Register 66, 5001-5193.

[3] Particle Measurement Programme (PMP), Light-duty Inter-laboratory Correlation Exercise (ILCE_LD), Final report, GRPE-PMP-18-02, 2007.

[4] ISO/TC 22/SC 5/WG 2 N 195E. ISO/FDIS 16183 – Heavy Duty Engines – Measurement of gaseous emissions from raw exhaust gas and of PM using partial flow dilution systems under transient test conditions; 2002-02-07.Reference 3,

[5] July 2008, The University of Novi Sad, Doctor degree thesis: Development of measurement method for measurement and verification of ultra fine particles from diesel engine emission, Technical faculty ``Mihajlo Pupin`` in Zrenjanin

[6] m-PSS, www.vandfna.com/**MICROPSS**-brochure.pdf

[7] AVL M.O.V.E PM PEMS 494 ,US EPA APPROVED COMBINATION OF REAL TIME SOOT AND INTEGRAL PM MEASUREMENT FOR IN-USE TESTING, AVL MSS

[8] Dekati DM-230, Mass Correlation of Engine Emissionswith Spectral Instruments www.idc-online.com/technical_references/pdfs/.../engineemissions.pdf ,
Dekati ETaPS www.testing-expo.com/europe/06txeu_conf/pres/.../tikkanen.pdf

[9] Horiba OBS TRPM manual v1.0 www.horiba.com

[10] SEMTECH PPMD manual www.sensors-inc.com/semtech_ppmd.htm.

[11] D.Booker, Sensor‟s, Inc., www.sensors-inc.com/semtech_ppmd.htm.

[12] Inter-Laboratory Correlation Exercise: Framework and Laboratory Guide, UN-GRPE PMP, Phase 3, Inf. Doc. No. GRPE-PMP-14-1, 2005.

[1] THE PARAMETER DETERMINATION OF THE CRANKSHAFT DYNAMICAL MODEL

Ivan Filipović, *Faculty of Mechanical Engineering Sarajevo*
Aleksandar Milašinović, *Faculty of Mechanical Engineering Banja Luka*

UDC: 620.175.22:621.436-233.1

Abstract

Crankshaft torsional vibration of the internal combustion engine has the most influence on the structural dimensioning of he crankshaft. In recent years increasing attention is paid to the diagnosis of the internal combustion engine through the evaluation of the angular speed variation of the crankshaft's. The angular speed variation of the crankshaft's is a consequence of contributions due to the rigid body motion and due to the torsional vibration of the crankshaft. In order to the crankshaft mathematical model that represent real dynamical system to give correct response it is necessary that model describe real dynamical process and that all input parameters, which are take a part in the model, are determined correctly. Determination of the torsional stiffness coefficient is a very demanding task, because of the complexity of boundary conditions. This paper presents a new approach for determining the torsional stiffness coefficient of a crank. By using this method, the real boundary conditions of the crankshaft of the diesel engine are considered, and the results obtained are reliable and confirmed by experiment.

Key words: torsional stiffness coefficient, crank of the crankshaft, diesel engine.

ODREĐIVANJE PARAMETARA DINAMIČKOG MODELA KOLENASTOG VRATILA

UDC: 620.175.22:621.436-233.1

Rezime: Torzione oscilacije koljenastog vratila motora sus predstavljaju najvažniji segment u definisanju konstruktivnih parametara koljenastog vratila. Posljednjih godina sve se više istražuje mogućnost dijagnostike rada motora na osnovu analize trenutne ugaone brzine koljenastog vratila. Promjenljivi dio ugaone brzine koljenastog vratila se sastoji iz kretanja koljenastog vratila kao krutog tijela i torzionih oscilacija. Da bi matematički model koji reprezentuje stvarni dinamički sistem davao korektne rezultate neophodno je: da model dobro opisuje fizičku suštinu procesa i da su parametri, koji figurišu u modelu, tačno određeni. Određivanje koeficijenta torzione krutosti koljena koljenastog vratila je veoma težak zadatak zbog složenosti graničnih uslova. U ovom radu se daje novi pristup definisanju krutosti koljena koljenastog vratila. Predloženi metod uzima u obzir realne

[1] Received: September 2010. Primljen: septembar, 2010.god.
Accepted: December 2010. Prihvaćen: decembar, 2010.god.

granične uslove rada koljenastog vratila dizel motora, a rezultati dobijeni proračunom se dobro slažu sa eksperimentom.

Ključne riječi: koeficijent torzione krutosti, koljeno koljenastog vratila, dizel motor.

THE PARAMETER DETERMINATION OF THE CRANKSHAFT DYNAMICAL MODEL

Ivan Filipović [1]*, Aleksandar Milašinović*

UDC: 620.175.22:621.436-233.1

INTRODUCTION

Reciprocating machines usually are provided with crank mechanisms to transform the reciprocating motion of the pistons into the rotating motion of the shaft. The crankshaft is subject to strong dynamic problems, among which torsional vibration is usually the most important.

A crankshaft is subjected to periodic dynamic loads, generating vibrations and stresses that must be quantified to ensure the structural integrity of the component. Today, due to technical, commercial and environmental requirements, internal combustion engines (ICEs) must operate with high cylinder pressures and the components must be optimized for the best performance. Modern calculation methods allow for the precise determination of stress levels in the crankshaft's critical regions, as well as evaluation of the fatigue strength. Thus, it is possible to consider design margins that ensure sufficient reliability to avoid structural failures of the components.

On the one hand, the intensity of torsional vibration has a crucial influence on crankshaft dimension and, on the other hand, the motion of the crankshaft, which is directly connected to torsional vibration, is the basis for combustion diagnostics [1, 13]. This important role of the IC engine's torsional vibration requires the development of both experimental methods for measuring torsional vibration and mathematical models for predicting torsional vibration. For the successful application of a mathematical model describing the torsional vibration of a crankshaft, it is necessary to know the parameters of the mathematical model (moment of inertia, stiffness coefficient, damping coefficient, and torque), and the boundary conditions. This paper contributes to a more realistic description of the torsional vibration system's parameters, especially the crankshaft torsional stiffness coefficient.

For torsional vibration analysis of the reciprocating machines, it is necessary to replace the real system with an equivalent dynamic model of the crankshaft in the most realistic way. The general scheme of the crankshaft's equivalent dynamic model with *n* lumped masses is shown in Fig. 1.

A multi-body extension of the torque balancing equation [8] may be expressed as

$$\mathbf{J}\ddot{\boldsymbol{\alpha}} + \mathbf{K}\dot{\boldsymbol{\alpha}} + \mathbf{C}\boldsymbol{\alpha} = \mathfrak{m}_g(\boldsymbol{\alpha}) - \mathfrak{m}_{in}(\boldsymbol{\alpha}) - \mathfrak{m}_t(\boldsymbol{\alpha}) - \mathfrak{m}_k(\boldsymbol{\alpha}) \tag{1}$$

[1] Corresponding author e-mail: *filipovic@mef.unsa.ba*, *Faculty of Mechanical Engineering Sarajevo, Vilsonovo Šetalište 1, Sarajevo*

where the dot notation stands for element-wise differentiation. **J; K** and **C** are symmetric matrices referred to as the mass, stiffness and damping matrices respectively. These matrices are all of size $n \times n$, where n is the number of lumped masses. It is customary to refer to **J** as mass matrix, even though for a torsional system it contains the inertia coefficients. The damping elements are modelled as viscous damping, i.e. the damping torque is proportional to angular velocity, $\dot{\boldsymbol{\alpha}}$. Stiffness and damping elements interconnected between adjacent lumped masses are here referred to as relative, and if connected between a mass lump and a non-rotating reference, absolute. The non-rotating reference is further referred to as ground. For modelling of an engine crankshaft, typically both absolute and relative damping elements are used, but only relative stiffness elements since the crankshaft is free to rotate about its axis.

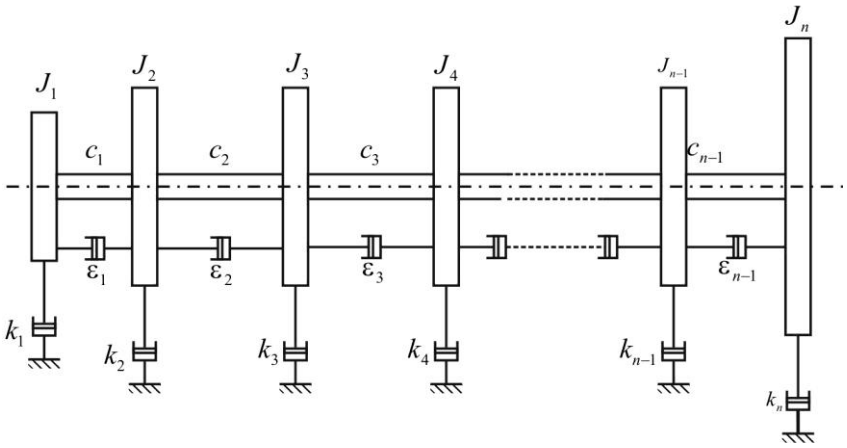

Figure 1: *Schematic diagram of the torsional dynamic model of the crankshaft*

Determination of the crankshaft torsional stiffness coefficient can be reduced to determining the torsional stiffness coefficient of simple cylindrical parts, and determining the torsional stiffness coefficient for a single crank of the crankshaft [3, 5, 12]. Determination of the torsional stiffness coefficient of the crank is a demanding task, because of its complex geometry and the difficulties in determining its boundary conditions. As is well known, there are three approaches to evaluating the torsional stiffness coefficient of a crank: experimental evaluation, application of semiempirical methods, and application of the FEM. The experimental method is expensive and a very demanding task. The problems are accurate measurement of the cranktwistangle and correct boundary conditions. Therefore, the experimental method is rarely used. The semiempirical method is based on semiempirical equations given by many workers [5, 6]. These equations are based on the empirical data and experimental results and are used for stiffness coefficient approximations. Today, the FEM is the most widely used method for determining the torsional stiffness coefficient. Determination of the torsional stiffness coefficient using any of the previously mentioned methods is a very demanding task, because of the complexity of boundary conditions. This paper presents a new approach for determining the torsional stiffness coefficient of a crank.

PARAMETER OF THE CRANKSHAFT MATHEMAICAL MODEL

Using modern computer-aided design (CAD) software, it is possible to derive the polar moment of inertia of lumped masses from the geometric representation. Based on drawings of all those parts of IC engines influencing the equivalent dynamic model of the crankshaft, solid models were created and moments of inertia computed. This approach is more accurate than the approximate methods given in reference [6], or even experimental methods, and thus the error has been minimized.

In the past, the effects of the internal combustion engines variable inertia were considered to be negligible and were disregarded from the calculations. Recently, these secondary effects were verified and checked and they are responsible per many crankshaft structural failures. In [8] was studied the effect of the non-constant moments of inertia on torsional vibration calculations. The introduction of functions taking into account the variation of the inertia over the crank throw angular position shall be considered, mainly in cases of large displacement engines, where the masses of the piston and connecting rods are significantly large when compared to the other components of the system. In this case it is possible neglected variation of the polar moment of inertia [8].

Although the response of the system in conditions far from resonance can be computed from an undamped model, the response at resonance can be obtained only after the damping of the system has been evaluated, and the precision of the results is strictly dependent on the precision with which damping is known. Because the resonant conditions are usually the most dangerous, this part of the dynamic analysis is important, and the difficulty in estimating the damping is one of the factors limiting the usefulness of the dynamic analysis and the need of resorting to extensive experimentation. In [8] is given method of parameter estimation of the damping in resonance condition.

The most widely used approaches for determining the crank torsional stiffness coefficient are semiempirical equations and the FEM. The total twist angle consists of the torsional twist angle of the main and crankpin journals, and the bending angle of the crankshaft crank's web. A simplified crankshaft's crank model, with cylindrically shaped main and crankpin journals and with the web of a parallelepiped shape, is used to derive semiempirical equations. Many researchers have tried to consider a real shape for the crank by implementing their equations for the torsional stiffness coefficient of a simplified crankshaft's crank with some correction factors. In this paper, the present authors have analysed the crankshaft's crank of a four-cylinder diesel engine, type TAM BF 4 L 515 C. Fig. 2 shows predictions for the torsional stiffness coefficient of a simplified single crank of the crankshaft, determined by semiempirical equations [6], and by the FEM using two different boundary conditions.

A solid model of a crankshaft's crank has been made in order to compare the FEM and semi empirical equations. The unsupported crank of the crankshaft was analysed first (Fig. 3). The obtained results agree well with those obtained by semiempirical equations, as can be seen from Fig. 2.

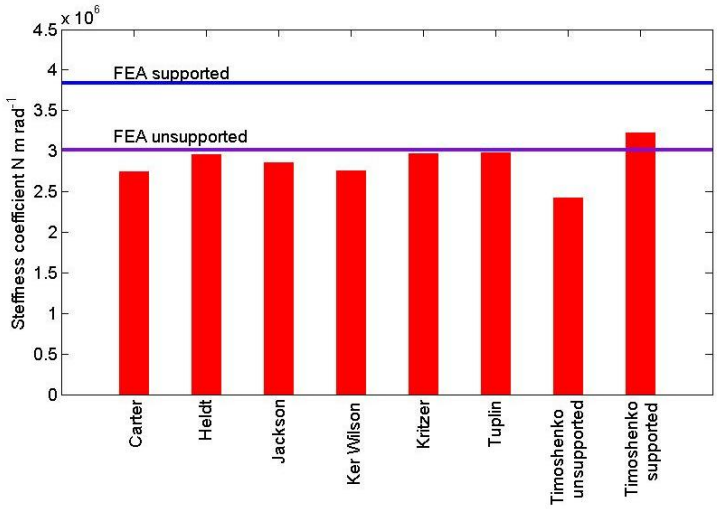

Figure 2: *Torsional stiffness coefficients of the crank predicted by the traditional approach (semiempirical equations) and finite element analysis (FEA)*

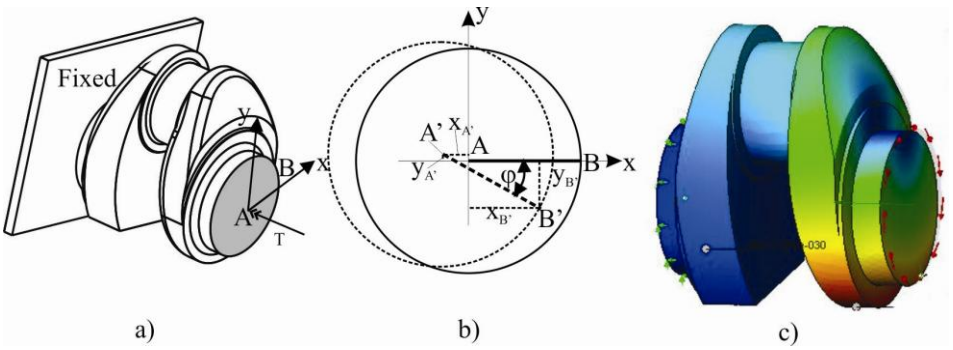

Figure 3: *The unsupported crank of the crankshaft: (a) sketch of the crank fixed at the left-hand side and loaded by the torsional moment T on the right-hand side; (b) the movement of the highlighted surface in the x–y plane due to action of the moment T; (c) corresponding FEM analysis*

However, the predicted torsional stiffness coefficient does not match the actual value, since the boundary conditions are unrealistic. Movement of the right main journal axis, which is unsupported, occurs (Fig. 3). The crank fixed at the left-hand side and supported without any clearance at the right-hand side was analysed next (Fig. 4). In this case the torsional stiffness coefficient is about 25 per cent higher than the stiffness coefficient of the crank with unsupported right journal, which is very close to the prediction of semiempirical models (maximum 8 per cent dissipation was found (Fig. 2)). It can, therefore, be concluded that the semiempirical equations given in the literature and corrected according to actual engine data match the boundary conditions of the unsupported right main journal, as presented in Fig. 2. Similar results are obtained for other analysed diesel engines. Two

cases have been studied by the presented FEM analysis of the crank torsional stiffness coefficient: first, the crank fixed at the left-hand side with unsupported main journal at the right-hand side; second, the crank fixed at the left-hand side with supported main journal without clearance at the right-hand side.

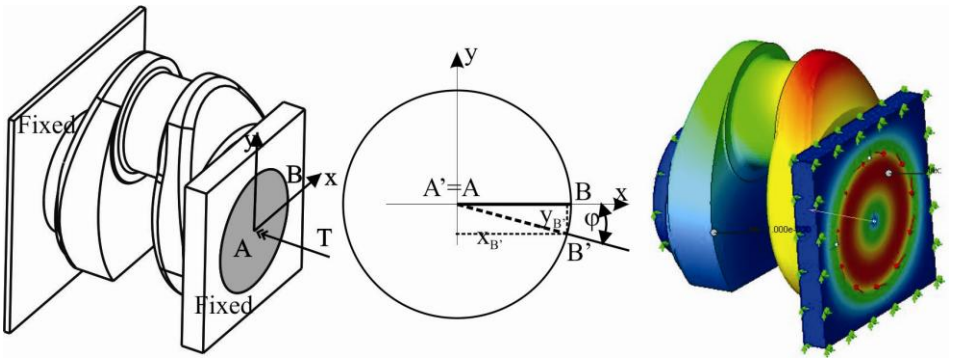

Figure 4: *The supported crank of the crankshaft without clearance: (a) sketch of the crank fixed on the left-hand side and supported without clearance at the right-hand side and loaded by the moment T; (b) the movement of the highlighted surface in the x–y plane due to action of the moment T; (c) corresponding FEM analysis*

These two cases represent theoretically extreme cases of the crankshaft's actual boundary conditions. The actual boundary conditions of the crankshaft are between these two extremes and they change during the working cycle. In addition to the dimensions of the crankshaft, the working conditions of the engine have the greatest influence on the actual boundary conditions.

RESULTS AND DISCUSSION

A four-stroke four-cylinder turbocharged diesel engine with air cooling (engine type TAM BF 4 l 515 C) was experimentally investigated. Those engine parameters important for torsional vibration analysis of the crankshaft were measured. These parameters are the crankshaft instantaneous rotational speed at the free end of the crankshaft (pulley), in-cylinder combustion pressure, and engine torque. All these parameters were measured simultaneously at different engine speeds and loads. The crankshaft speed at the free end was measured by the optical encoder. A detailed description of the experimental set-up and analysed results has been given in reference [8]. The characteristics of the tested engine are presented in Table 1.

Table 1: *Type Tested engine characteristics (engine type TAM BF 4 L 515 C)*

Property	Symbol	Value	Unit
Engine power	*P/n*	150 at 2150 r/min	kW
Engine torque	*T/n*	787 at 1500 r/min	Nm
Bore diameter	*D*	125	mm

Property	Symbol	Value	Unit
Stroke	*s*	145	mm
Crank radius	*r*	0.0725	m
Length of the connection rod	*l*	0.237	m
Firing order		1–3–4–2	–
Reciprocating mass	m_A	4.6	kg
Rotating mass	m_B	2.6	kg

The polar moments of inertia of the equivalent torsional vibration system's lumped masses had to be known in order to perform torsional vibration analysis of the tested engine. The polar moments of inertia of the lumped masses were determined (with high accuracy) using CAD software (Solid Works). Measurements were performed for various engine operating regimes under maximum engine load, by gradually increasing the engine speed from 1000 r/min to 2250 r/min using 50 r/min steps. The angular speed variation of the crankshaft's free end was calculated on the basis of the known angular step of the optical encoder, and the measured time necessary to run the distance, i.e. the angular step, as

$$\omega = \frac{\Delta\alpha}{\Delta t} \tag{2}$$

The crankshaft speed variation may be expressed in a Fourier series as

$$\omega = \omega_0 + \sum_{j=1}^{\infty}(\omega_{c_j} \cos\frac{j\omega_0 t}{2} + \omega_{s_j} \sin\frac{j\omega_0 t}{2}) \tag{3}$$

where ω_0 is the average (constant) angular speed, and ω_{c_j} and ω_{s_j} are the *j* th-order harmonic components of the crankshaft's speed. The angular position of the crankshaft's free end is obtained by integrating equation (3) to give

$$\alpha = \omega_0 t + \sum_{j=1}^{\infty}\left(\frac{2\omega_{c_j}}{j\omega_0}\sin\frac{j\omega_0 t}{2} - \frac{2\omega_{s_j}}{j\omega_0}\cos\frac{j\omega_0 t}{2}\right) \tag{4}$$

The second term in equation (4) consists of contributions due to the rigid body motion and due to the torsional vibration of the crankshaft [1, 12]. Fig. 5 show, only as examples, the harmonic analysis and the synthesis of the measured speed variation of the crankshaft's free end for two engine operating regimes (n=1000 r/min and n=1850 r/min).

The main harmonic components of the gas pressure torque act in the same direction for all cylinders and it is possible to sum their amplitudes algebraically. The main harmonic of tenth order is dominant at 1850 r/min, and it excites the torsional vibrations of the crankshaft (Fig. 5). At 1000 r/min, however, the second- and fourth-order main harmonics

are dominant. The frequencies of these harmonics are lower than the natural frequency of the system. These harmonics are caused by mechanical excitation due to combustion and inertial forces and represent the rigid body motion of the crankshaft.

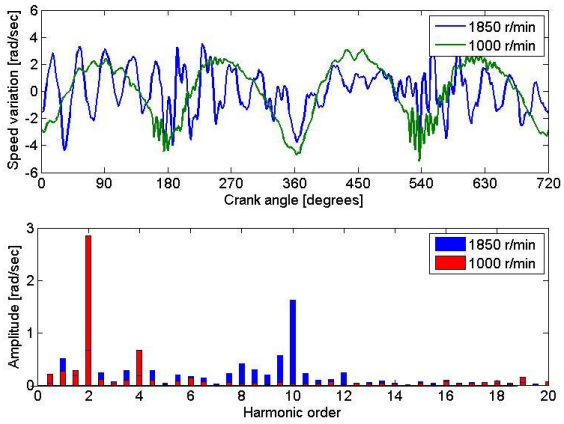

Figure 5: *(a) Harmonic synthesis and (b) analysis of speed variation of the crankshaft's free end at 1000 r/min and 1850 r/min*

An amplitude spectrum of the crankshaft free end's speed variation is shown in Fig. 6. The main harmonics 10, 12, and 14 are within the engine's operating range. Other harmonics (just the most important, 8.5, 9, 9.5, 10.5, and 11.5 are shown) are also present within the engine's operating range. These harmonics are caused by crankshaft torsional vibration. It is possible to determine the natural frequency of the torsional vibration system, by analysing the results shown in Fig. 6. However, taking into account the fact that the engine speed was varied using 50 r/min steps, and by considering experimental error, it is more convenient to predict the natural frequency interval rather than its exact value.

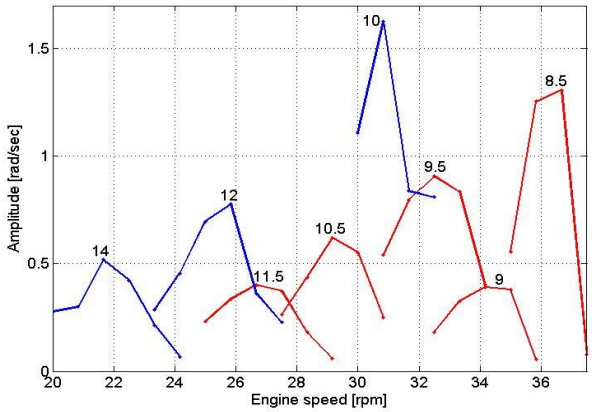

Figure 6: *The amplitude spectrum of the speed variation of the crankshaft's free end as a function of engine speed within the engine's operating range (engine type TAM BF 4 L 515 C)*

DETERMINATION OF A CRANK TORSIONAL STIFFNESS

The stiffness coefficient of the crank may be determined if the first natural frequency is known, which is the basic concept of the suggested indirect method. A mathematical model of the system's free vibration is given by the equation

$$\mathbf{J}\left(J_1, J_2, ..., J_n\right)\ddot{\boldsymbol{\varphi}} + \mathbf{C}\left(c_1, c_2, ..., c_n\right)\boldsymbol{\varphi} = \mathbf{0} \tag{5}$$

where $\boldsymbol{\varphi}$ is the vector of the crankshaft's torsional vibration.

The research was performed purposely on the engine without the torsional vibration damper. The stiffness coefficient of the torsional vibration damper is non-linear and could induce the wrong conclusions. The solution for the ordinary differential equation system (5) is of the type $\boldsymbol{\varphi} = \mathbf{q}e^{\lambda t}$, where λ is the natural frequency of the system and $\mathbf{q}$ is the amplitudes vector. The characteristic equation of the relevant eigenproblem is then

$$\left(\lambda^2\mathbf{J}\left(J_1, J_2, ..., J_n\right) + \mathbf{C}\left(c_1, c_2, ..., c_{n-1}\right)\right)\mathbf{q} = \mathbf{0} \tag{6}$$

Specifically, non-trivial solutions for $\mathbf{q}$ are possible if, and only if, the determinant of the linear homogeneous equation system (6) is equal to 0; thus

$$\det\left[\lambda^2\mathbf{J}\left(J_1, J_2, ..., J_n\right) + \mathbf{C}\left(c_1, c_2, ..., c_{n-1}\right)\right] = 0 \tag{7}$$

Equation (7) is known as the characteristic equation of the system. When all parameters of the system (J_1, J_2, …, J_n, c_1, c_2, …, c_{n-1}) are known, then the solution of the characteristic equation (7) yields the n-1 natural frequencies of the system ($\lambda = 0$ is also a solution), which is a common approach to this problem. In this case, however, the parameters of the system are not completely known, thus an indirect solving method was applied [2, 8, 10]. The first natural frequency is known from the harmonic analysis of the speed variation of the crankshaft's free end. Such a set of parameters can now be found, so that the first natural frequency will solve equation (7). Not all the parameters are unknown. The moments of the lumped masses' inertia were computed using CAD software. Thus only n-1 unknown torsional stiffness coefficients of the crankshaft section have to be found. If it were possible to determine all the n-1 natural frequencies, then a system of n-1 non-linear equations could be obtained, which would yield the n-1 unknown stiffness coefficients.

However, determining the natural frequencies of the torsional vibration systems of the second, third, and higher modes is impossible for the following reasons:

1. The natural frequencies of the second, third, and higher modes are very high (e.g. the second frequency of the analysed torsional vibration system exceeds 4730 1/s); therefore, only very high orders of excitation torque (torques of orders 20 and higher in this case) are within the engine's operational range.
2. The excitation torque orders of 20 and higher have very low amplitude, which is very difficult to obtain accurately.

The differences in the stiffness coefficients of the crank are very low, therefore, it is possible to assume that the crank stiffness coefficients are equal ($c_{k_1} = c_{k_2} = ... = c_{k_l} = c_k$) in most cases. When the cranks of the crankshaft are not equal, then the stiffness coefficients of any cranks may be expressed as a function of the stiffness coefficient of the reference crank, where the first crank is selected as the reference crank. The stiffness coefficients of all other sections (*j*) of the crankshaft, which are cylindrical, can be calculated using the equation

$$c_j = \frac{G\pi D^4}{32l} \tag{8}$$

The torsional stiffness coefficient of the crankshaft section *i*, which is between two lumped masses and consists of *j* subsections with different stiffness coefficients, can be calculated from the equation

$$\frac{1}{c_i} = \sum_j \frac{1}{c_j} \tag{9}$$

After some rearrangements using equations (8) and (9) the characteristic equation (7) becomes an (*n*-1) th-order polynomial with c_k as a variable. The solutions of this polynomial are *n*-1 c_k values. In the mathematical sense, each of these values is the solution of equation (7). However, by considering their physical meaning, it is possible to determine a single solution, which satisfies the nature of the process and, therefore, represents the stiffness coefficient of the system. It has already been shown that the correct stiffness coefficient lies within a range of theoretically predicted extreme values. The lower extreme is the stiffness coefficient of the crank with an unsupported main journal and the upper extreme is the stiffness coefficient of the crank with a fixed main journal.

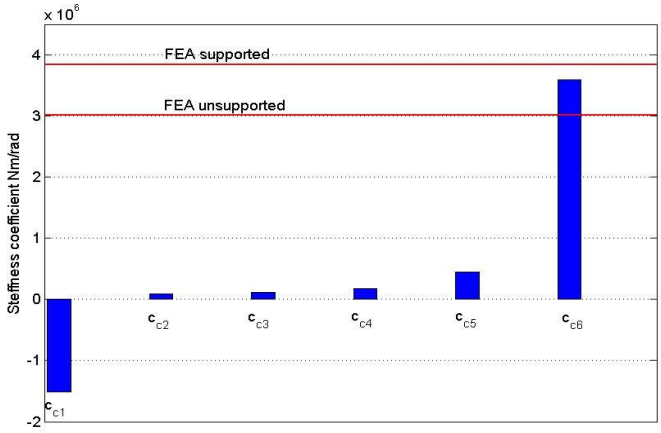

Figure 7: *The torsional stiffness coefficients of the crank determined by the indirect method and FEM (FEA, finite element analysis)*

As can be seen from Fig. 7, only one of the solutions of equation (7) is within this range. In this particular case it is, therefore, the correct stiffness coefficient. This value is about 8 per cent lower than the stiffness coefficient of the supported main journal without clearance (Fig. 4), and almost 16 per cent higher than the stiffness coefficient of the unsupported main journal (see Fig. 3). The actual stiffness coefficient of the crank is closer to the stiffness coefficient of supported main journal without clearance, which may be expected owing to the very small clearance of the main journal.

Based on the obtained results of the calculation of the torsional stiffness (c_{kus}) of the crank of the engine crankshaft with free right-hand end and with the torsional stiffness c_{ks} of the crank of the crankshaft with the main bearing journal without clearance on the right-hand end of the crankshaft by the FEM and experimental results obtained indirectly by measuring torsional vibrations, it is suggested that the equation for calculating the stiffness of the crank of the engine crankshaft in real working conditions is

$$c_k = c_{ks} B\left(c_{ks} - c_{kus}\right) \tag{10}$$

The constant *B* represents a coefficient that reflects portions of torsion and bending of the crank of the engine crankshaft load with torque in real working conditions. For certain groups of internal combustion engines the constant B can be adopted as constant, without regard to some construction differences of the crank of the crankshaft. Analysing the results of calculations of stiffness of the crank of the crankshaft for the engine used in this paper, as well as use of similar analysis for two six-cylinder diesel engines with net powers of 140 kW and 210 kW, the value of the constant B=0.35 is obtained. This coefficient can be accepted for the category of diesel engine for heavy-duty vehicles and buses.

CONCLUSIONS

- The variation of the crankshaft's speed is determined by the variation of the external torque and the dynamic response of the crankshaft structure. For steady state operation conditions, the lower harmonic components of the gas pressure torque do not excite torsional vibrations.
- The amplitude of the half harmonic order of the crankshaft's speed may be correlated to the extent of the non-uniformity in the contribution of a cylinder to the total engine torque.
- Accurate determination of the system's parameters, and in particular the torsional stiffness coefficient of crank, is necessary in order to perform reliable quality and quantity analyses of the crankshaft's torsional vibration system.
- The accuracy of traditional empirical methods used for determining crank torsional stiffness coefficient is limited owing to the complex shape of the crank and the sophisticated boundary conditions (loads and supports of the journals).
- It is difficult to determine the actual boundary conditions and to predict the crank stiffness coefficient correctly by the FEM; therefore, the indirect method presented in this paper is suggested for determining the crank torsional stiffness coefficient
- In the case of a diesel engine used in heavy-duty vehicles, equation (10) is acceptable for calculating the torsional stiffness of the crank of the crankshaft in

real working condition with the constant B=0.35.

- For defining the coefficient B using the indirect method, in the case of certain groups of engines, a more suitable is the method of non-contact measurement of torsional vibration shown in this paper, in relation to traditional methods of measurements of torsional vibrations.
- The calculation methodology presented here can be applied to several types of ICEs from spark ignition to diesel engines, in-line or 'V' types, and 2- or 4-stroke engines, taking into account the correct ignition timing and sequence. However, for large displacement engines, e.g. marine ICE, other effects such as influence of large oscillating parts (non-constant polar moments of inertia) cannot be disregarded in the calculations.
- If the frequency of the lowest major harmonic order of a multi-cylinder engine is low with respect to the first natural frequency of the shafting, for the whole speed range of the engine, the shafting behaves dynamically like a rigid body.

ACKNOWLEDGMENTS

The authors acknowledge the technical support of the Laboratory for internal combustion engines, Faculty of the Mechanical engineering, University of Maribor.

REFERENCES

[1] Bombek, G., Milainović, A., Filipović, I., and Hribernik, A.: "Determination of torsional vibrations of a diesel engine crankshaft", In Proceedings of the Conference on Innovative automotive technology (IAT'05), 21–22. April 2005, Bled, Slovenia, pp. 236–242,

[2] Filipović, I. and Jankov, R.: "Modern approach to measurement and analysis of the IC engines parameters", In Proceedings of the International Scientific Symposium on Retracing the puch track, September 2001, Ptuj, Slovenia, pp. 126–132,

[3] Filipović, I., Doleček, V., and Bibić, Dž.: "Modeling and the analysis of parameter in the torsional-oscillatory system equivalent to the diesel engines in transport vehicles", Journal of Mechanical Engineering, Vol. 51, No. 12/05, iss. 488, 2005, pp 786-797,

[4] Filipović, I.: "IC engine dynamics and vibration", 2007, Faculty of Mechanical Engineering, University of Sarajevo Sarajevo, Bosnia and Herzegovina,

[5] Genta, G.: "Vibrations of structures and machine", 1993, Springer-Verlag, Berlin,

[6] Hafner, K. E. and Maass, H.: "Torsionsschwingungen in der Verbrennungskraftmaschine", 1985, Springer-Verlag, Berlin,

[7] Milašinović, A., Filipović, I., and Hribernik, A.: "Mathematical model for choosing the flywheel of an IC engine", In Proceedings of the 8th International Conference on Accomplishments in electrical and mechanical engineering -DEMI 2007, 2007, Banja Luka-Bosnia and Herzegovina, pp. 767–775,

[8] Milašinović, A.: "Mathematical modeling and experimental investigation of nonlinear torsional vibration of crankshaft of IC engine. PhD Thesis, April 2007, University of Banja Luka-Bosnia and Herzegovina,

[9] Schagerberg, S. and McKelvey, T.: "Instantaneous crankshaft torque measurements-modeling and validation", SAE paper 2003-01-0713, 2003,

[10] Serban, R. and Freeman, J. S.: "Identification and identifiability of unknown parameters in multibody dynamic systems. Multibody System Dynamics J., 2001, Vol. 5, pp. 335–350.

[11] Shabana, A.: "Dynamics of multibody systems", 2005, Cambridge University Press, Cambridge,

[12] Taraza, D., Henein, N. A., and Bryzik, W.: "Determination of the gas-pressure torque of a multicylinder engine from measurements of the crankshaft's speed variation", SAE paper 980164, 1998.

[13] Taraza, D., Henein, N. A., and Bryzik, W.: "The frequency analysis of the crankshaft's speed variation: a reliable tool for diesel engine diagnosis", ASME Journal of Engineering for Gas Turbines and Power, 2001, Vol. 123, pp. 428–431.

[14] Taraza, D.: "Quantifying relationships between the crankshaft's speed variation and the gas pressure torque", SAE paper 2001-01-1007, 2001.

[1] MODELLING AND ANALYSIS OF FORCES IN THE CONTACT OF A VEHICLE PNEUMATIC WHEEL AND A ROAD SURFACE WHEN THE VEHICLE PASSES OVER AN IRREGULARITY

Sreten Simović, *Faculty of Mechanical Engineering in Podgorica, Montenegro*

UDC: 692.012.3: 519.872

Abstract

The paper gives an analytic and experimental analysis of forces in the contact of a vehicle pneumatic wheel and a road surface when a vehicle passes over a defined road surface irregularity. A mathematical model of dynamical behaviour of the system suspension-wheel-road surface on the basis of which is formed a mathematical model for computer simulation is established in this paper. The validity of the established mathematical model of the system is confirmed by comparison of the simulation results with the results obtained experimentally.

Key words: vehicle, wheel, irregularity, mathematical model, simulation.

MODELIRANJE I ANALIZA SILA U KONTAKTU PNEUMATIK-PODLOGA PRI KRETANJU VOZILA PREKO NERAVNINA PODLOGE

UDC: 692.012.3: 519.872

Rezime: U radu je data analitička i eksperimentalna analiza sila u kontaktu pneumatik-podloga pri prelasku vozila preko definisane neravnine podloge. U radu je postavljen matematički model dinamičkog ponašanja sistema elastično oslanjanje-točak-podloga na osnovu kojeg je formiran matematički model za računarsku simulaciju. Upoređenjem rezultata simulacije sa rezultatima dobijenim eksperimentalnim putem potvrđena je validnost postavljenog matematičkog modela sistema.

Ključne riječi: vozilo, točak, neravnina, matematički model, simulacija.

[1] Received: September 2010. Primljen: septembar, 2010.god.
Accepted: November 2010. Prihvaćen: novembar, 2010.god.

MODELLING AND ANALYSIS OF FORCES IN THE CONTACT OF A VEHICLE PNEUMATIC WHEEL AND A ROAD SURFACE WHEN THE VEHICLE PASSES OVER AN IRREGULARITY

Sreten Simović [1]

UDC: 692.012.3: 519.872

INTRODUCTION

Driving comfort, lifetime of components and systems and power efficiency of a vehicle, besides functional capability of the vehicle, represent the most important indicators of the vehicle quality.

The achievement of these requirements, expecially when the vehicle travels in off-road conditions, is very complex. Thereat, with regard to the interconnection between the wheel and the road surface, the compatibility of characteristics of the vehicle systems and characteristics of the road surface is of special importance .

The dynamic forces generated when the vehicle passes over an irregularity influence vehicle stability and driveability as well as vehicle elements lifetime considerably. On the other hand, these forces have preferential influence on the loading of the road surface which is the factor with main influence on the road surface lifetime and quality. Also, these forces influence the road structures loading and oscillating, [2, 5].

In terms of the above mentioned, modelling and analysis of forces in the wheel-road contact while a vehicle travels over road irregularities, which is the theme of this paper are significant for solution of tasks connected with the selection of parameters of particular vehicle systems so that they are in accordance with stated quality demands, [8].

THE INFLUENCE OF ROAD IRREGULARITIES ON A VEHICLE

A road, with irregularities on the road surface, has a great influence on the loading of the vehicle transmission and suspension system. Passing of the vehicle over any kind of road surface is characterized with permanent variation of forces at the wheel-road contact point. The forces generated at the wheel-road contact point mainly depend on the vehicle speed, the road surface irregularities as well as on the vehicle construction, especially its suspension system, [6]. These variations are induced by the shape and dimensions of the irregularities, on the one hand, and characteristics of the vehicle systems on the other.

The statement that irregularities of the road surface have unfavourable, impulsive, influence on the vehicle systems, and therefore on the vehicle suspension, transmission and steering

[1] Corresponding author e-mail: sretens@ac.me, Faculty of Mechanical Engineering in Podgorica, Džordža Vašingtona bb, 81000 Podgorica, Montenegro

system, can be given on the basis of the fact that the vehicle wheel is, at the same time, part of these three vehicle systems. Whereby we could not forget the fact that forces generated between the wheel and the road have the primary importance for accomplishing the primary vehicle function which may be represented as a need for generating sufficient intensity of these forces to maintain the vehicle stability and driveability. On the basis of the aforesaid it is obvious that any variation of these forces in the wheel-road contact will be reflected on the dynamical behaviour of the three above mentioned systems. This influence couldn't also be neglected, when a vehicle passes over modern, relatively flat roads. Even the best roads in terms of irregularities are characterized by random irregularities in the area around the intermediate value, which can be a source of random vibrations of the vehicle structure. Thus, when the vehicle travels over a relatively good road, the loading of the vehicle axis isn't constant but fluctuates up to ±15%. This variation is called as dynamic load, [3], Figure 1.

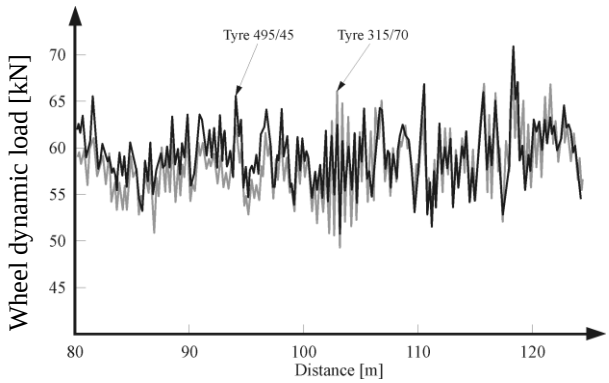

Figure 1: *Wheel dynamic load at rolling along flat road surface*

However, in the analysis of the forces in the wheel-road contact what represents a great difficulty is the complexity of the vehicle structure and the complex characteristic of the wheel behaviour on an irregularity, so that even nowadays we don't have a complete and satisfactory theory describing the process, [4]. This analysis is especially complex when we take into consideration that the time of the passing of the wheel over individual irregularities is very short and so that their influence on the vehicle may widely fluctuate depending on the vehicle characteristics, e.g. wheel pneumatic tyre, pressure and the characteristics of the vehicle suspension system. Modelling of the pneumatic wheel for the situations when the wheel passes over an irregularity is especially problematic, also, because of a great pneumatic tyre compression which might occur in the process, possible nonlinearities of the tyre structure and complex characteristics of deformation, [9].

While calculating the lifetime of the vehicle elements, that is its vehicle transmission, we must take into consideration that this system is at the same time influenced by:

- the engine drive moment, the moments of the losses in transmission, the moments of the resistance forces of driving, the loading of the flywheel masses of the engine and transmission and

- the loading induced by the transient processes caused by the road surface profile, variation of the engine moment and oscillating of the resistance moments.

The vertical and horizontal force which react at the contact point on the vehicle wheel, i.e. the road surface, can be separated in two components, [1]:

- static loading, induced by the vehicle and load mass, which depends on the geometry and the vehicle mass arrangement and suspension system and
- dynamical loading of the wheel or axis, induced by the vehicle vibration due to the road roughness.

In the diagrams shown in Figure 2 is presented the experimentally obtained change of the vehicle semishaft moment and the change of the relative position in suspension when the vehicle passes over an irregularity. We can notice that when the vehicle passes over a relatively short triangular irregularity in the vehicle transmission a great oscillation of the moment occurs, which in this particular case exceeds the value of the moment on semishaft at the moment of achieving contact between the wheel and the irregularity by over 80%. We can also notice the intensive change of the relative position in suspension. It is obvious that this intensive change is induced by the change in the vertical and horizontal force at the wheel-road contact point.

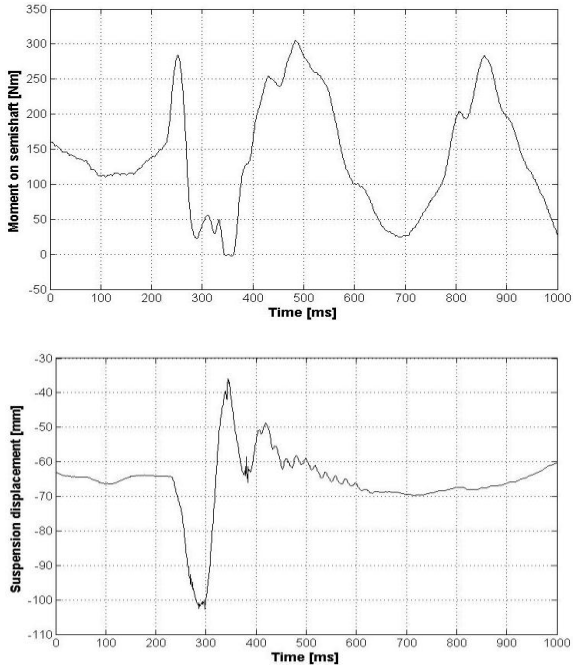

Figure 2: *Change of drive moment on semishaft and suspension relative movement*

On the basis of the fact that the process of passing of the wheel over an irregularity is a distinctly nonstationary process, we can conclude that the best way for defining functional dependences of the changes of a particular vehicle system characteristics will be an experimental investigation.

This approach is shown in literature [4], where the author conducts an analysis of the intensity of the generated vertical and horizontal forces on the wheel and then performs an analysis of the efective road grade. In this approach the author also performs an experimental testing with the wheel rotating freely on a fixed axis, whereby different values of vertical and horizontal loadings are induced. The wheel rolls over the surface and passes over the defined irregularities. This approach shows that through an analysis of the vertical and horizontal forces we can define the character of the change in values of these forces and that the change may be mathematically represented in a satisfactory manner, Figure 3.

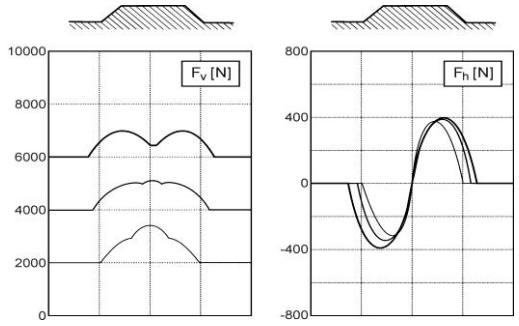

Figure 3: *Forces generated on a trapezoidal obstacle*

However, the experimental testing conducted by the author of this paper, in comparison to the approach shown in literature [4], leads us to the conclusion that in real conditions considerably different character of force change is obtained because the real conditions of vehicles use are considerably different from the conditions in which the above mentioned experiment was performed. In real conditions the wheel is driven by an engine, the wheel is an elastic element and as part of unsuspended mass it is movable in a vertical direction, and above it, according to the usual simplified approach, there is also movable suspended mass, Figure 4. The appropriate method of analysis and the example of modeling of the simplified suspension system is performed and validated earlier and presented in an earlier paper and therefore will not be presented here, [7].

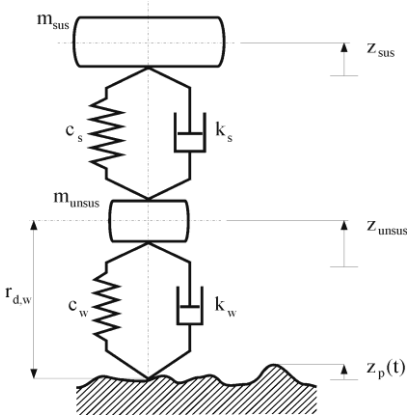

Figure 4: *Scheme of a quarter vehicle suspension model*

In order to set functional dependences while accepting the approach shown in literature [4], it is necessary to provide experimentally obtained data in real conditions of the vehicle use.

Due to the complexity of the analysis and the necessity of detailed defininig of loading, besides the description of the vertical and horizontal forces, to perform an analysis of the dynamical behaviour of transmission we must also define a change of the wheel moment, because in contrast to other analysis, for instance the analysis of the suspension system where also must be the value of the vertical force is of the most prevailing influence, in this case a position of the contact point between the wheel and the road surface which have prevailing influence on the value of the wheel moment, must also be defined, Figure 5.

Besides that having in mind the need for detailed definig of the influence of the characteristics of separate vehicle systems it is important to obtain posibilities for defining values of the generated wheel forces in dependence of suspension system characteristics.

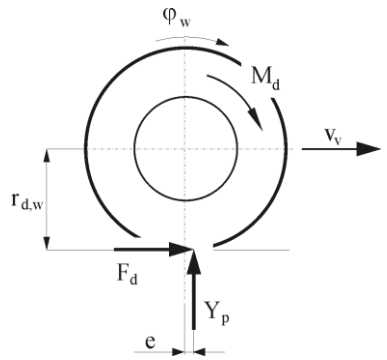

Figure 5: *Loading of vehicle wheel*

THE MATHEMATICAL MODEL OF THE DYNAMICAL BEHAVIOUR

In distinction from the case when a vehicle passes over a flat surface, a dynamical analysis of the process of passing over an uneven road surface becomes considerably more complex. The following text offers an example of analysis for the situation when a wheel passes over a triangular irregularity of a defined geometry for a quarter car model.

The equation of dynamical equilibrium for a vehicle in the horizontal direction has the following form:

$$\sum F_x = 0, \qquad F_{pog} - \sum F_{otp} = 0$$

and:

$$F_d = F_f + F_v + F_\alpha + F_{in}$$

After linearization of the precedent equation it is obtained that the following condition should be fulfilled at any time:

$$F_{d,0} + \Delta F_d = F_{f,0} + \Delta F_f + F_{v,0} + \Delta F_v + F_{\alpha,0} + \Delta F_\alpha + F_{in,0} + \Delta F_{in}$$

After the analysis of the individual members of the above equation and considering the observed analysis we can state that:

- For the equation member which represents the wheel rolling resistance, F_f, and is dependent on the value of the vertical reaction, Y_p, and coefficient of the rolling resistance, f, we can conclude that for the values of the coefficient f we cannot use the values for this coefficient defined for the case when the wheel travels along a flat surface because when the wheel passes over an irregularity a notable change in position of the vertical reaction force on the wheel occurs thereby changing the parameter e, which means that we can't express this resistance explicitly.
- The member which defines the change in air resistance, F_v, can be neglected because in this case traveling speed is relatively small.
- For calculating the member which represents the road inclination resistance, F_α, we cannot use the conventional calculation method because in this case the vehicle travels along a flat surface with an irregularity which is first only under the front wheel and then only under the rear wheel, with phase shift dependent on the vehicle speed and the wheelbase. In this case vehicle rotation around its transverse axis occurs. We must also consider that the wheel is an elastic element. On that basis we can conclude that in this case we cannot use the angle of irregularity as the value for the road surface inclination.
- As for the member representing the inertial characteristics of the vehicle, F_{in}, on the basis of the available experimentally gained data regarding the time of passing of the wheel over the irregularity, we can reach a conclusion that in this case the traveling speed remains almost constant. Because of that we can neglect the inertial parameter of the vehicle translatory mass since the influence of the vehicle mass is of no practical significance.

Based on the above mentioned we may conclude that in this case we need to analyze only the rolling ressistance caused by the irregularity i.e. parameter which represents the horizontal distance from the wheel axis and the contact point, the and equivalent wheel deformation in radial direction.

Considering the aim of this analysis, i.e. the elaboration which, as a result, will have characteristics of the dynamical behaviour of vehicle transmission, besides the presentation of the transmission elements as elastic elements with equivalent masess, stiffness and damping, we must also give a description of the behaviour of the driving wheel as the last part of the vehicle transmission system, Figures 4 and 5.

The dynamical equation of the wheel moment for its axis of rotation, using indices shown in Figure 5, has the following form:

$$\sum M = 0, \qquad M_d = J_w \cdot \ddot{\varphi}_w + Y_p \cdot e + F_d \cdot r_{d,w}$$

namely: M_d – wheel drive moment,
J_w – wheel momentum of inertia,
$\ddot{\varphi}_w$ – wheel angular acceleration,
Y_p – vertical reaction force,
e – distance of vertical reaction from wheel vertical axis, e.g. wheel-road equivalent reaction point,
$r_{d,w}$ – vertical distance from wheel axis and equivalent reaction point.

The momentum equation of the driving wheel we can also express as a function of the tangential force on the wheel, $F_{T,w}$, Figure 5, so we have:

$$\sum M = 0, \qquad M_d = J_w \cdot \ddot{\varphi}_w + F_{T,w} \cdot r_{e,w}$$

Where the parameter $r_{e,w}$ represents the radius which defines the distance from the point of action of the resultant force at the wheel-road surface contact from the wheel axis.

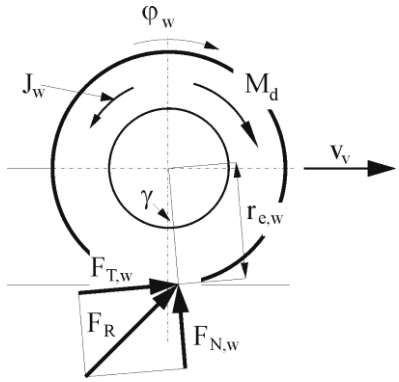

Figure 6. *Wheel loading presented with tangential and normal force at contact point*

The parameters $F_{T,w}$ and $r_{e,w}$ can be calculated from the following equations based on Figure 7:

$$F_{T,w} = Y_p \cdot \sin\gamma + F_d \cdot \cos\gamma$$

$$F_{N,w} = Y_p \cdot \cos\gamma + F_d \cdot \sin\gamma$$

$$r_{e,w} = r_0 - \frac{F_{N,w}}{c_{r,w}}$$

In the above equation paramter $c_{r,w}$ represents the wheel stiffness in the radial direction and for this parameter, for the reason of simplification, the mean value will be accepted, since this value varies within a wide range depending on the manner the contact between the wheel and the irregularity is realized. This characteristic can only be obtained by experimental investigation of the wheel stiffness for different situations of contact implementation.

As is mentioned before, for defining of the position of the equivalent contact point between the wheel and the road surface we must define two parameters; namely the angle of contact point relative to the wheel vertical axis, γ, and then the distance between the wheel axis and the contact point, $r_{e,w}$. The equation which defines the change of parameter γ is obtained in the following manner:

$$M_d = J_w \cdot \ddot{\varphi}_w + \left(Y_p \cdot \sin\gamma + F_d \cdot \cos\gamma\right) \cdot \frac{F_N}{c_{r,w}}$$

If we disregard the inertial member and introduce a substitute for member F_N we get:

$$M_d = \left(Y_p \cdot \sin\gamma + F_d \cdot \cos\gamma\right) \cdot \frac{Y_p \cdot \cos\gamma + F_d \cdot \sin\gamma}{c_{r,w}}$$

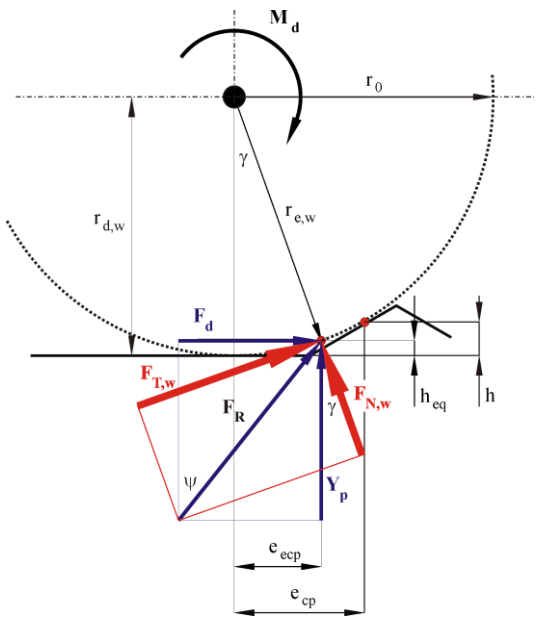

Figure 7: *Geometric dependence of the wheel forces*

For the needs of a more detailed analysis of the pneumatic tyre behaviour which also include characteristics of individual parts of the vehicle wheel, the stiffness and damping of

the wheel rim and the pneumatic tyre, the wheel is represented by two mass scheme shown in Figure 8, on the basis of which, after linearization, the following equations can be derived.

$$\Delta M_d = J_{rim} \cdot \Delta\ddot{\varphi}_{rim} + \left[c_{pn} \cdot \left(\Delta\varphi_{rim} - \Delta\varphi_{pn}\right) + k_{pn} \cdot \left(\Delta\dot{\varphi}_{rim} - \Delta\dot{\varphi}_{pn}\right)\right] \cdot \left(r_{rim} + \frac{r_{out} - r_{rim}}{2}\right) +$$

$$+ \left[c_{pn} \cdot \left(\varphi_{rim} - \varphi_{pn}\right)_0 + k_{pn} \cdot \left(\dot{\varphi}_{rim} - \dot{\varphi}_{pn}\right)_0\right] \cdot \left(\frac{\Delta r_{rim} + \Delta r_{out}}{2}\right)$$

$$\left[c_{pn} \cdot \left(\Delta\varphi_{rim} - \Delta\varphi_{pn}\right) + k_{pn} \cdot \left(\Delta\dot{\varphi}_{rim} - \Delta\dot{\varphi}_{pn}\right)\right] \cdot \left(r_{rim} + \frac{r_{out} - r_{rim}}{2}\right) +$$

$$+ \left[c_{pn} \cdot \left(\varphi_{rim} - \varphi_{pn}\right)_0 + k_{pn} \cdot \left(\dot{\varphi}_{rim} - \dot{\varphi}_{pn}\right)_0\right] \cdot \left(\frac{\Delta r_{rim} + \Delta r_{out}}{2}\right) = J_{pn} \cdot \Delta\ddot{\varphi}_{pn} +$$

$$+ \left[c_{out} \cdot \left(\Delta\varphi_{pn} - \Delta\varphi_{out}\right) + k_{out} \cdot \left(\Delta\dot{\varphi}_{pn} - \Delta\dot{\varphi}_{out}\right)\right] \cdot r_{out,0} +$$

$$+ \left[c_{out} \cdot \left(\varphi_{pn} - \varphi_{out}\right)_0 + k_{out} \cdot \left(\dot{\varphi}_{pn} - \dot{\varphi}_{out}\right)_0\right] \cdot \Delta r_{out}$$

$$\Delta F_T = c_{out} \cdot \left(\Delta\varphi_{pn} - \Delta\varphi_{out}\right) + k_{out} \cdot \left(\Delta\dot{\varphi}_{pn} - \Delta\dot{\varphi}_{out}\right)$$

namely: J_{rim}, J_{pn} – rim and pneumatic tyre momentum of inertia,

φ_{rim}, φ_{pn}, φ_{out} – angle of rotation of wheel rim, pneumatic tyre and traction surface,

F_T – wheel tangential force acting on traction surface,

c_{pn}, k_{pn} – stiffness and damping coefficient of pneumatic tyre,

c_{out}, k_{out} – stiffness and damping coefficient of wheel traction surface,

r_{rim}, r_{out} – radius of rim and wheel traction surface.

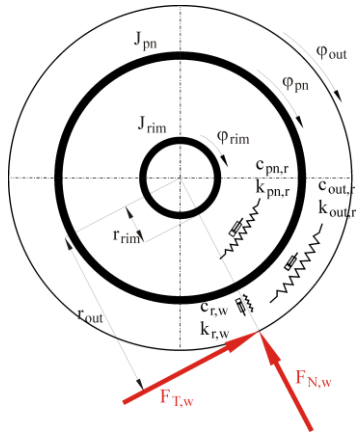

Figure 8: *Wheel represented as two mass dynamical system*

THE SIMULATION OF THE DYNAMICAL BEHAVIOUR

In the aim of presenting the explained approach schematically and verification of the possibilities of simulation of the dynamical behaviour of the vehicle transmission here will be presented an example of simulation in the case case when a wheel passes over an irregularity with a defined geoometry. As an input in the system experimentally obtained data is used; namely, momentum on the vehicle semishaft [10], the relative position of suspension and the vertical and horizontal wheel forces on the irregularity. Since we must obtain values for wheel forces for the entire period of simulation, i.e. for the period when the wheel is not on the irregularity, it is accepted that these values are constant and equal to the values of these forces just before the wheel comes in contact with the irregularity. This approach has its justification in the fact that, as we can notice, there is a relatively small change in the relative position of the suspension elements after the wheel passes over the irregularity, compared to the change during the period of passing over the irregularity.

The experiment was performed on a real vehicle equipped with pneumatic tyres 175/70 R13, with 2 bar pressure in the pneumatic under the traveling speed of approximately 20 km/h. The model uses the values of other characteristics also obtained by additional experiments. Primarily these are the wheel inertia, the stiffness of suspension and the stiffness of the wheel on a flat surface and in two cases of the wheel-irregularity contact, one for the wheel-irregularity contact at two points and the other when wheel is positioned exactly on the irregularity. The irregularity is triangular with height of 57 mm and length of 190 mm.

Because of the impossibility of presenting the complete dynamical model of transmission components, in the following figure is presented a scheme of a complete model of the vehicle transmission used for simulation.

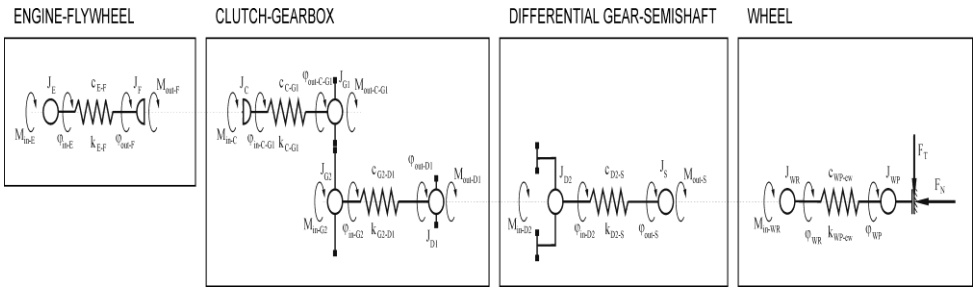

Figure 9: *Simulation scheme*

Dynamical behaviour of vehicle transmission components is described by suitable differential equations. After performing the computer simulation in program Matlab, module Simulink, while using experimental data for the achieved wheel vertical and horizontal forces, shown in Figure 10, as well as the change in the relative position of suspension elements, Figure 11, the characteristics of dynamical behaviour of vehicle transmission are obtained and presented in Figure 12. The changes of the equivalent values for the angle and distance of the contact point from the wheel axis are presented in Figures 13 and 14.

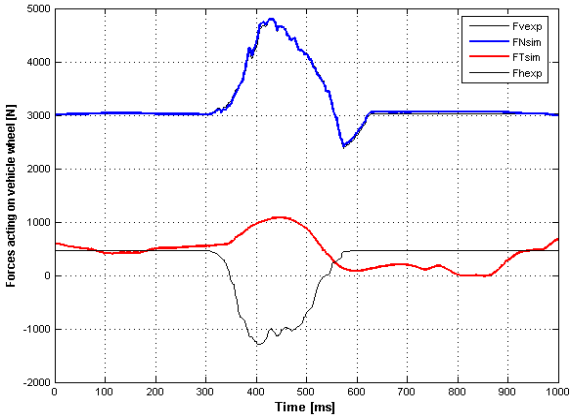

Figure 10: *Change of the wheel vertical and horizontal forces with wheel tangential and normal force*

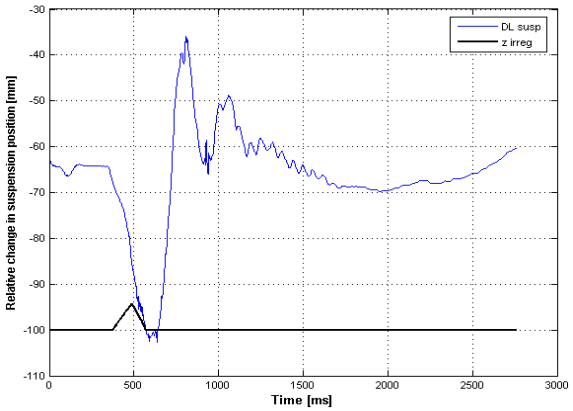

Figure 11: *Change of the relative position of the suspension assembly*

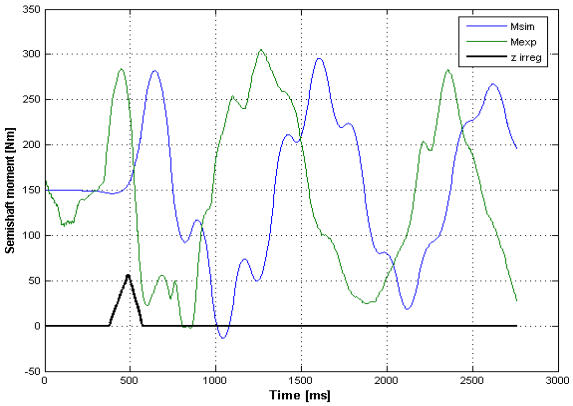

Figure 12: *Change of the drive moment on the semishaft*

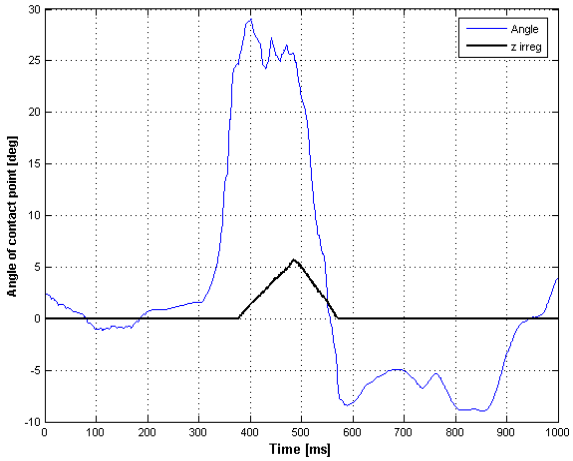

Figure 13: *Change of contact point angle*

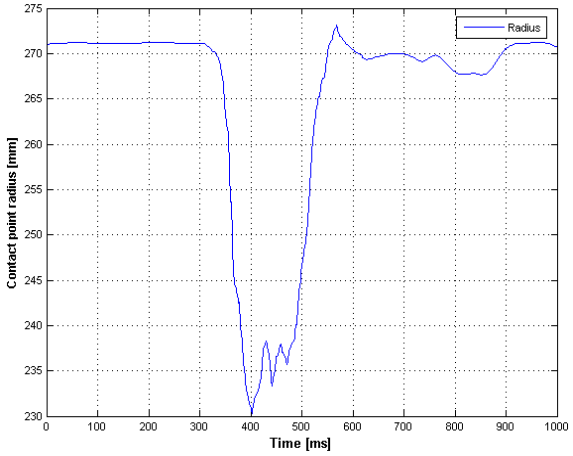

Figure 14: *Change of the contact point radius*

CONCLUSION

On the basis of the experiments conducted and the simulation described in this paper, it can be concluded that for the situation when a vehicle travels along an uneven road surface the characteristic of wheel force change is very complex .

The results of the experiments and simulation presented in the paper are in a very good accordance. Based on the above said, we can conclude that a relatively simple analytical model of the vehicle drive system, on which the computer simulation is performed, has a comparative importance that this approach has significance for the analysis of the behaviour of a vehicle passing over irregularities.

For a complete analysis of the vehicle transmission loading in order to obtain its elements lifetime prediction a large number of different tests must be performed with different types of irregularities, which is the subject of further research of the author of this paper.

ACKNOWLEDGMENTS

I would like to take this opportunity to express my sincere gratitude to Professors Radan Durković and Aleksandra Janković for their kind support and help on preparing this paper as well as in the overall work on my doctoral dissertation, part of which is this paper.

REFERENCES

[1] Cebon, D.: "Interaction between Heavy Vehicles and Roads", L. Ray Buckendale Lecture, SAE 1993, SP-951, SAE Trans 930001

[2] Hedrick, K., Yi, K.: "The Effect of Alternative Heavy Truck Suspensions on Flexible Pavement Response", University of California, Transportation Center, Working paper No 46, 1991

[3] Huhtala, M., Halonen, P., Sikiö, J.: "Measurements on Dynamic Effects of Dual and Wide Base Single Tyres", Technical Research Centre of Finland (VTT), COST-334 REPORT

[4] Pacejka, H. B.: "Tyre and Vehicle Dynamics", Second edition, Butterworth-Heinemann, 2006, Oxford

[5] Pesterev, A. V., Bergman, L. A., Tan C. A.: "Pothole-Induced Contact Forces in a Simple Vehicle Model", Journal of Sound and Vibration, 2002

[6] Potter, T. E. C., Collop, A. C., Cole, D. J., Cebon, D.: "A34 Mat Tests: Results and Analysis", CUED/C-MECH/TR 61, 1994

[7] Simović, S., Durković, R.: "Theoretical and Experimental Analysis and Modelling of Vehicle Suspension System Kinematic", XXII International Automotive Conference Science and Motor Vehicles 2009, JUMV 2009, University of Belgrade, Faculty of Mechanical Engineering, Belgrade, 2009

[8] Glišović, J., Miloradović, D., Dunkić, A., Radonjić, R.: "Development of a software for modeling of vehicle excitation due to the road roughness", MVM – Volume 23, Number 3, Kragujevac, 1997

[9] Potincu, G., Neagu, E.: "Models and methods for determination of efforts between tyre and undeformable road", MVM – Volume 24, Number 2, Krahujevac, 1998

[10] Simić, D., Slavković, D.: "Određivanje dinamičkih reakcija tla putničkog automobila", MVM – saopštenja (VIII) 43/44, Kragujevac, 1982.

[1]ALGORITHM FOR 3D SURFACE RECONSTRUCTION BASED ON POINT CLOUD GENERATED BY OPTICAL MEASURING TECHNIQUES

Milan Blagojević, Miroslav Živković, *Faculty of Mechanical Engineering, Kragujevac, Serbia*

UDC:004.896:62

Abstract:

Free form surface can be accurately reconstructed only on the basis of a large number of measuring points. This measuring project is more complex, and the digitization is realized by both TRITOP and ATOS optical measurement systems. TRITOP was performed very precisely position measuring of uncoded reference points and adapters. ATOS digitize complete surface of object. A result of digitization is detailed triangulated mesh.

Depending on application, creating of the model's surface is carried out with introduction of certain assumptions and approximations, based on knowledge of model's processing technology. The presented procedure generates digitized object's surface, approximated by NURBS.

Key words: Optical 3D digitization, 3D surface reconstruction, Reverse Engineering, Product development, CAD/CAM/CAE.

ALGORITAM ZA REKONSTRUISANJE 3D POVRŠINE NA OSNOVU OBLAKA TAČAKA DOBIJENOG OPTIČKIM MERNIM TEHNIKAMA

UDC:004.896:62

Rezime: Free form površina može biti precizno rekonstruisana jedino na osnovu velikog broja mernih račaka. Ovaj merni projekat je nešto kompleksniji, a digitalizacija je vršena optičkim mernim sistemima ATOS i TRITOP. TRITOP omogućava precizno merenje položaja adaptera i nekodiranih referentnih tačaka. ATOS digitalizuje kompletnu površinu objekta. Rezultat digitalizacije je detaljna trougaona mreža.

Zavisno od primene, rekonstrukcija površine modela vrši se uvođenjem izvesnih pretpostavki i aproksimacija, na osnovu poznavanja tehnologije proizvodnje modela.

[1] Received: October 2010. Primljen: oktobar, 2010.god.
Accepted: December 2010. Prihvaćen: decembar, 2010.god.

Prikazanom procedurom generiše se površina objekta digitalizacije, aproksimirano NURBS površinom.

Ključne reči: Optička 3D digitalizacija, rekonstrukcija 3D površine, reverzni inženjering, razvoj proizvoda, CAD/CAM/CAE.

ALGORITHM FOR 3D SURFACE RECONSTRUCTION BASED ON POINT CLOUD GENERATED BY OPTICAL MEASURING TECHNIQUES

Milan Blagojević[1], *Miroslav Živković*

UDC:004.896:62

INTRODUCTION

In order to satisfy today's requirements in the functional, aesthetic and ergonomic reasons, products are mostly very complex shapes. Physical product designs like clay and other prototypes should be converted into solid models for making the required tooling. The new products or tools development are often based on already existing products, prototypes or physical models. They should be reconstructed in one of the CAD program in order to obtain a computer model suitable for further design, construction of tools and production preparation. Through the shown process, we extract the digital shape of any physical object. Classic measuring methods provide insufficient number of points for precise products surface reconstruction, because such free form surface can be accurately reconstructed only on the basis of a large number of measuring points. Non contact digitizing is done through optical measuring systems ATOS and TRITOP [1-3], which captures hundreds of thousands of points in a single shot of the object. A result of digitization is detailed poligonized mesh or point cloud, intersections, characteristic lines or other geometric elements. These measuring results provide very accurate computer reconstruction of shape, and so reduce development time and increase product quality. Reconstructed surface or volume models are loaded in standard formats in the CAD programs and further processed as needed.

In this paper, emphasis is specifically placed on accurate reconstruction of the physical model surface, which in some aspects may deviate from the principle of geometric proper reconstruction. This means that most areas are in fact a free form surfaces. From the standpoint of Reverse Engineering (RE), we are trying to describe a lot of sub-areas of the surface by the basic geometric entities: planes, sphere parts, cylinder parts, etc. In the parts processing, especially in fabrication of pressed parts, sub-areas of the surface resulting from flat sheet metal panels are not transformed in the precisely defined mathematical surface.

However, such a reconstructed surface of the physical model is very important, because real and very accurately describe the complex geometry of manufactured objects. The importance of their implementation is very noticeable in the finite element method, in which the use of these areas to create models that describe the geometry is made, not the ideal obtained by 3D modeling. In practice, it is known that very often geometric imperfections of the real model cause events that would not be caught observing the idealized model - CAD model.

[1] Corresponding author e-mail: blagoje@kg.ac.rs, Faculty of Mechanical Engineering, Sestre Janjić 6, Kragujevac, Serbia

3D DIGITIZING PROCESS

As example, we consider automotive industry part, figure 1. With other elements of the assembly is connected through the holes in the body. Because of that fact, it is necessary to record the exact 3D positions of the holes during digitizing process. Therefore, this measuring project was more complex, and the digitization is realized by both TRITOP and ATOS measurement systems. Optical measuring system TRITOP is performing very precisely measuring the position of uncoded reference points and adapters. ATOS sensor is then used to digitize the entire surface of the object of measurement. This method increases the accuracy of ATOS sensor for one size order.

3D digitizing by optical measuring system TRITOP

In order to meet requirements defined by both optical measuring systems, object is properly prepared for 3D digitization process. In this measuring project, measuring object is prepared from the point of its application for accurate determination of holes and adapters positions, as well as to generate a cloud of reference points that will be recognized by the ATOS sensor and used to calculate all sensor's positions. Measuring project must provide a precise determination of the coordinates of hole center, by placing the appropriate (sphere) adapter, and allow the determination of the position ATOS sensor in all individual measurements necessary to digitize the complete surface. In this way, measuring projects created by systems ATOS and TRITOP are located in the same coordinate system, which is very important for their usability in the quality process of reconstruction of the surface.

Figure 1: *Measuring volume prepared for optical measurements by optical measuring systems TRITOP (left) and ATOS (right)*

Measuring configuration of the optical measuring system TRITOP used in the digitization is given in Table 1.

Table 1: *Optical measuring system* TRITOP,
Measuring configuration: NIKON D200 + Optical Scale Bar 1000mm

TRITOP Photogrammetric Sensor	*NIKON D200*
TRITOP Scale Bars	*Optical Scale Bar 1000mm* *SG00243, Dist.0/1: 906.351mm, CrNi Steel at* 20^0C $16.2x10^4K^{-1}$ *SG00244, Dist.2/3: 907.577mm, CrNi Steel at* 20^0C $16.2x10^4K^{-1}$
Coded Reference Points	*15bit Coded Reference Points*
Application software	*TRITOP v6*

In order to accurately determine the position of holes and cylinders axis, special supplies - adapters is used. Figure 2 shows the hole adapter and its applications in this measuring project. It consists of semi-sphere, which the center is set very precisely by one uncoded reference point. Software is unable to self-identify this adapter, and for its use is necessary to define a plane around the hole where the hole located by applying uncoded reference points around. In addition, the cylinder adapter is used, which the software recognizes thanks to the unique layout of uncoded reference points on the adapter body, figure 3.

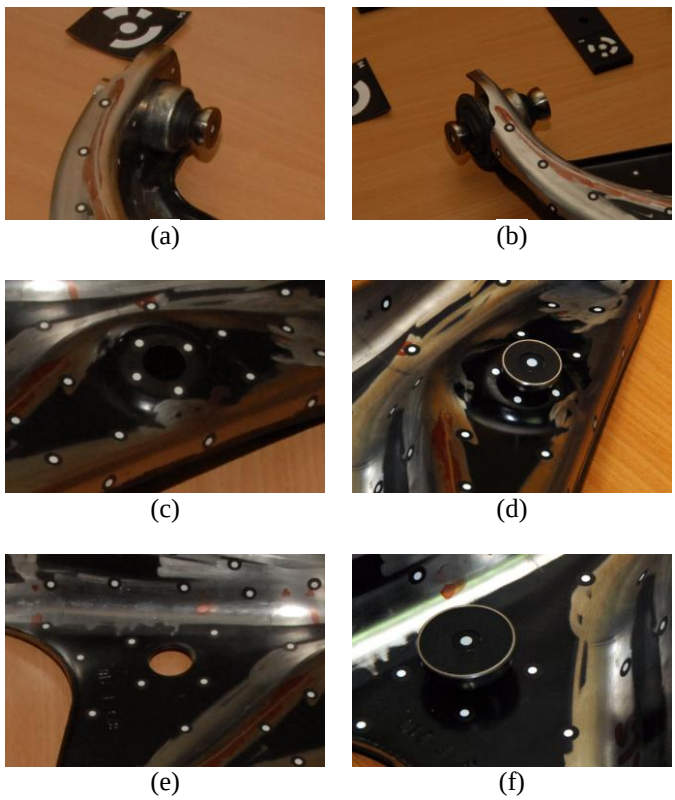

Figure 2: *Application of sphere adapters in digitizing project*

Based on the values of cylinder diameter, the software determines cylinder axis position. The common characteristic of all adapters is that they can move within the measuring volume, if it does not violate conditions necessary for the discharge of TRITOP measurements, especially violations of the relative layout of coded and uncoded reference points (mostly due to the measurement moving object within the measuring volume).

Measurement by optical measuring system TRITOP is performed making a series of images around the measuring object at angles of 45°, 75° and 90° in relation to the plane in which lies the measuring object and reference objects. As a rule, the first four measuring images, taken from the same place and relatively rotated around optical camera axis at angle of 90°, which should cover the entire measuring volume, is called calibration. During the processing of the measuring project, based on recorded images, software determines the system parameters and calculates the expected measuring error. If adapters move within the measuring volume, it is necessary to make the series, at least 3 measuring images, where software can see the adapter placed in the new position. Moved adapters is automatically recognized by the software and marked with adapter name followed by number of adapter's appearance.

Figure 3: *Application of cylinder adapters in digitizing project*

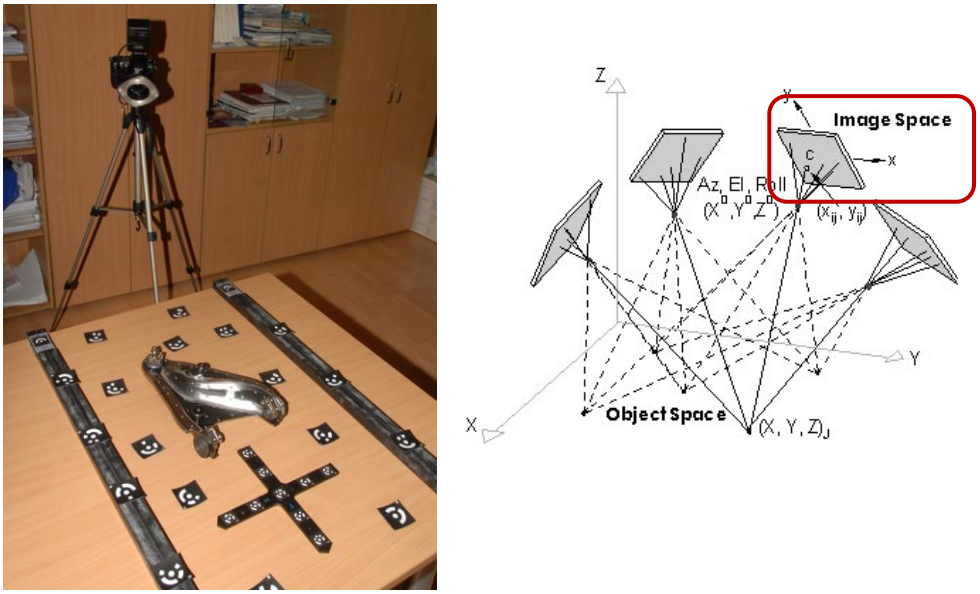

Figure 4: *Individual measurement by optical measuring system TRITOP*

The results of this measurement are shown in figure 5. Entity label shows coordinate of point placed on the hole axis. Figure 6 shows lines that represent the axis of the hole. Notice that the position of these lines will be taken into account on the basis of reference points through which lines pass (points 1063, 1070, 1101 and 1121), figure 6. The position of these points is read from the corresponding .REF file.

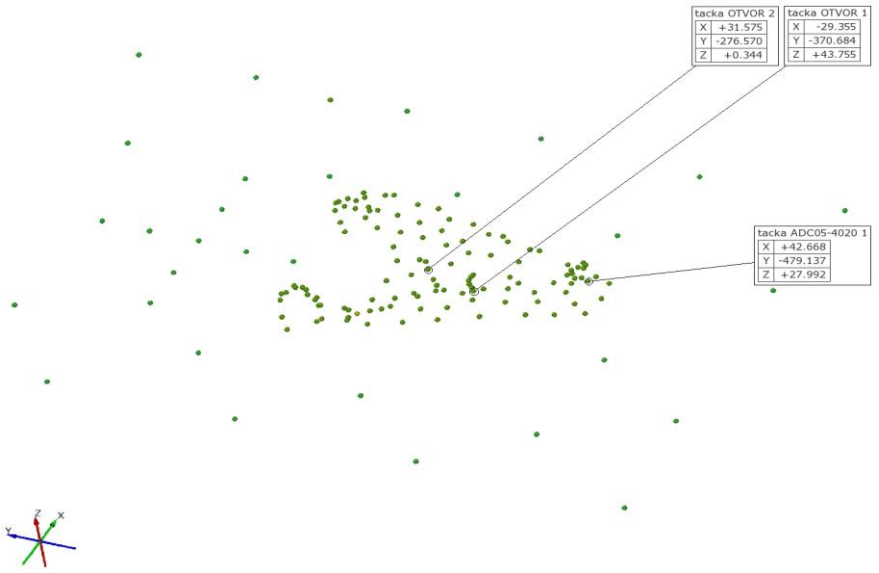

Figure 5: *Uncoded reference points*

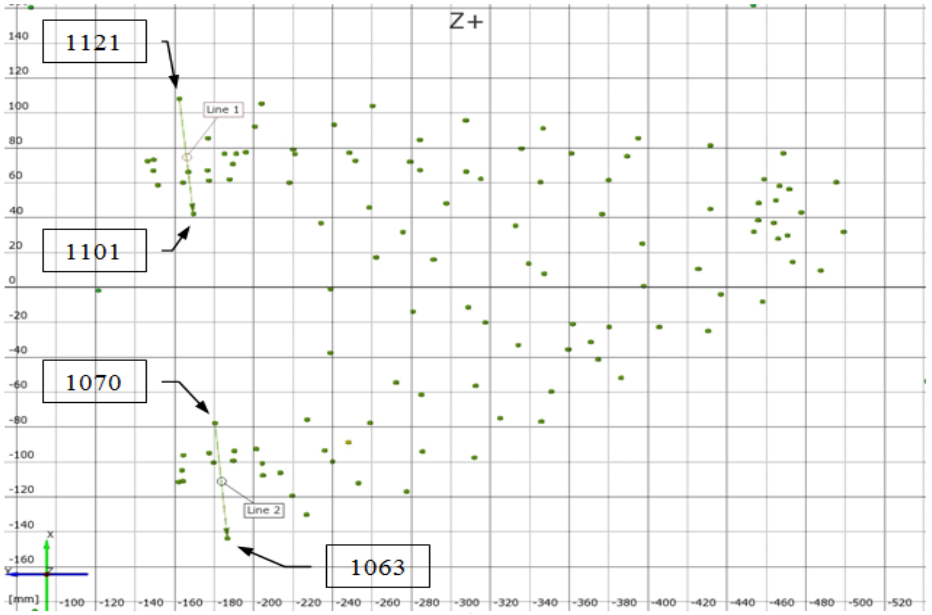

Figure 6: *Coordinates of characteristic points and adapters*

3D digitizing by optical measuring system ATOS

In order to successfully perform 3D digitizing process, it is necessary to properly perform all previous tasks. ATOS digitizing sensor calculates its 3D coordinates based on visible reference objects - uncoded reference points. Reference point diameter and strategy of points applying to object's surface are function measuring volume used. As the measuring object is not painted, its direct exposure to light source (projector) causes the appearance of too large illuminated (overexposed) areas of measuring images. In order to resolve this problem, the surface is sprayed by material which reduces the degree of reflection. This is done by applying spray titanium-dioxide (TiO_2) on the surface of the object to be digitized.

Based on dimensions of measuring object, required accuracy, and density of the point cloud, it is chosen appropriate measuring volume. The measuring volume is part of the space in front of the measuring sensor where whole measuring object or its part, is placed during the digitization, figure 7. To digitize objects larger than the selected measuring volume, it is necessary to move the object relative to the sensor. Throughout multiple individual measurements the entire area is recorded.

Configuration of measuring system for 3D digitizing ATOS, used in digitizing, is given in Table 2. In figure 7 is shown a single measurement of the model with ATOS measuring system and model after preparation for digitizing, with the set coded reference points after applying the spray to make surface is frosted.

Measuring process is carried out through sufficient number of individual measurements. All individual measurements are made at an angle 45°-60° relative to the plane in which lies the measuring object. In ATOS software positions of reference points applied to the object is known via .REF file that is imported to the software. Individual measurements are placed into the same coordinate system as is TRITOP measurement coordinate system.

Table 2: *Optical measuring system ATOS,*
Measuring configuration: ATOS II 400 + Calibration Panel 250

Sensor Configuration	*Measuring volume: 250x200x200 [mm x mm x mm]* *Reference point size: 3 [mm]* *Projector lense, focal length: 17 [mm]* *Camera lenses, focal length: 23 [mm]*
Calibration Object	*Calibration Panel 250* *CP20/MV250x200mm^2, SN: CP20/250/D05470,* *Aluminum 22.9x10^{-6}mmK^{-1}*
Application software	*ATOS v6*

Result of digitizing proces is point cloud. Point cloud is the set of points that "lie" on the surface of the digitized object, whose positions were calculated in relation to the coded reference points. Taking into account that the typical measurement consists of several individual measurements and on the fringes of the measuring volume position leads to distortion of recorded points (due to optical characteristics of the system), in certain areas

points are overlaped. Throughout the process of poligonization, the system automatically is re-calculating the position based on the captured images, adjust the positions and delete unnecessary items, with respect to the maximum page length limit while software constructs triangles between points.

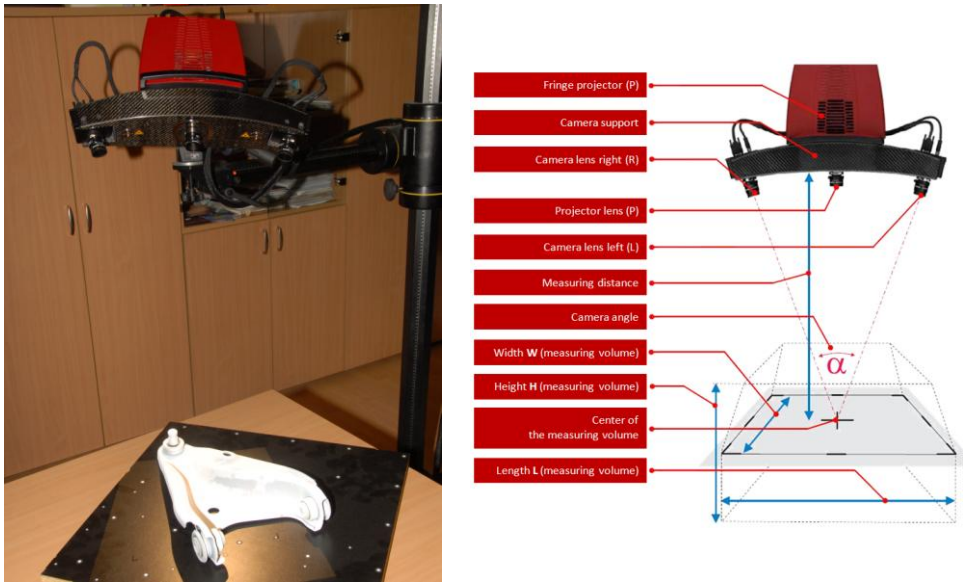

Figure 7: *Individual measurement by optical measuring system ATOS*

One of the poligonization parameters is the raster. Raster determines the level of detail to be displayed in the 3D object window, as well as the level of detail that will make during poligonization. For example, the value of 1:4 means that in areas of high curvature of every point, and in areas of low curvature of every fourth point is shown. For small objects of measurement should be used raster 1:4 or 2:8, and 4:16 for large objects or 8:32. Detailed 3D view imply its slower generation. For common measurement projects, it should be used the default values for the parameters of the project: 4:16. Final result is poligonized mesh.

Figure 8: *Poligonized mesh constructed over a generated point cloud*

Before poligonization model consists of 4 176 570 points. The resulting model consists of 152 636 points and 297 409 polygons. On the hard disk model occupies 796.9 MB of memory. The model describes the physical model of the scanned surface with an accuracy of 20μm.

3D SURFACE RECONSTRUCTION

Depending on application, creating of the model's surface implies the introduction of certain assumptions and approximations, based on knowledge of processing technology of model whose geometry is reconstructed. The process of generating NURBS surface consists of:

- procedures for point cloud processing (importing and filtering of points in point cloud, mesh generation, smoothing, cleaning, filling of holes on mesh, decimation and optimization) and
- procedures for generating smaller surface areas (creating and joining of 3D curves, basic patch creating, creating of surface's parts over patches, filleting, blending and joining of surface's parts).

3D surface reconstruction is performed in software CATIA V5. All necessary commands are placed in Workbenches under group Shape (Digitized Shape Editor, Quick Surface Reconstruction, Generative Shape Design, Free Style, and Automotive Class A).

Point Cloud Processing

Point cloud is imported in Workbench Digitized Shape Editor. Cleaning of mesh, removing spikes, discontinuities and other errors in point cloud is done in order to make regular mesh. Figure 9 shows point cloud after these operations. Next, poligonized mesh is generated, over resulting point cloud, figure 10. All these phases include some distortion in working data, so software ATOS and CATIA have compatibilities to compare mesh with source point cloud (which very precisely describes digitized surface) in form of labels, sections or complete deviation field.

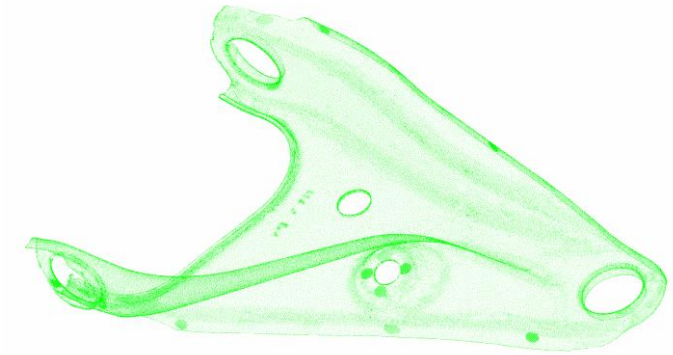

Figure 9: *Point cloud*

Figure 10: *Poligonized mesh constructed over a generated point cloud*

The model requires the accurate reconstruction of the position of the axis of holes, whose positions is known very precisely based on measurements carried out by optical measuring system TRITOP. That data is stored in .REF file, created by TRITOP software. Line 1 is determined by points 1101 (41.9003943; -169.647239; 26.4823138) and 1121 (107.838156; -162.653828; 25.6007972). Line 2 (see figure 4) is determined by points 1063 (-143.972816; -186.931743; 26.1068344) and 1070 (-77.9779967; -180.684895; 26.4785585). These coordinates are used during point creation (command Point in Workbench Generative Shape Design). Through that points, axis of holes is created, figure 11.

Figure 11: *Position of geometrical entities axis constructed based on TRITOP measurement data*

3D Surface Generating

The following steps are carried out over poliginized mesh. The same commands in different Workbenches have different options and are often necessary to pass from one Workbench to another in order to achieve maximum impact for some commands.

System of 3D lines over poliginized mesh is drawn, figure 12 (a). Notice that lines are limiting area that can be considered as to be flat. CATIA software offers many

opportunities for proper selection of the surface that are flat, by drawing curvature field of the surface or points deviation field in relation to the plane which best fit selected point. Lines that limit such areas are joined into one entity by command Join. Commands Fill and/or Fit create surface bounded by these lines, figure 12 (b).

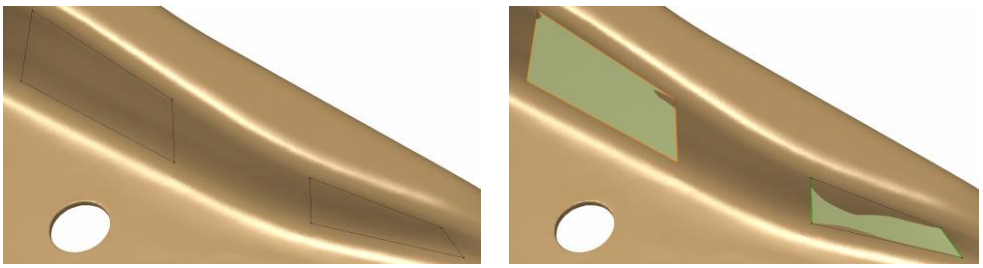

(a) (b)

Figure 12: *3D lines and surfaces bounded by these lines*

These surfaces, defined in this procedure until this moment, are merged with areas for which we assume as cylinders with large radius by command Free Style Blend Surface, figure 13 (a). Cylinders with a small radius are reconstructed by the command Styling Fillet, figure 13 (b). Now, we face with areas which basic mathematical surfaces can't define. It is so-called Free Form surface. Command Free Style Blend Surface restores such areas. In areas with no points, to reconstruct the surface command Multisections Surface is used, with border section and line leaders as parameters.

This is an iterative process and it is often necessary to return a few steps backwards in order to achieve the desired effect of a particular command.

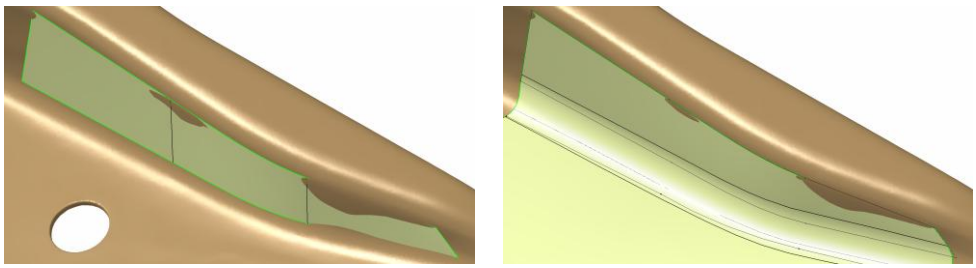

(a) (b)

Figure 13: *Phases in construction of patches over the triangulated mesh*

Figure 14 shows the parts of the total area, which are generated by previous process. All these sub-surfaces by merging produce surface that completely defines upper surface of whole digitized model, figure 15.

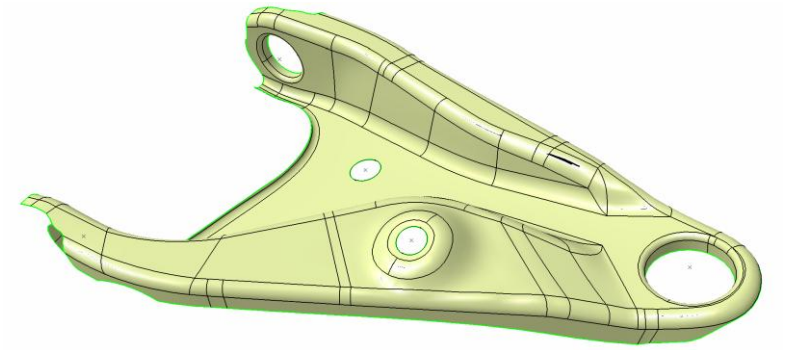

Figure 14: *Part of surface constructed over a poligonized mesh*

Figure 15: *Generated NURBS surface*

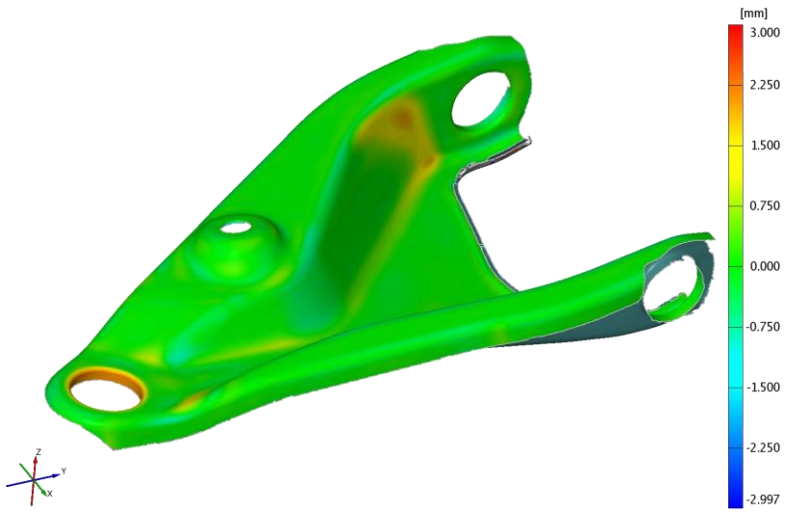

Figure 16: *Deviation field of generated surface in relation to reference (digitized) mesh*

Generated surface is imported in ATOS software to determine the deviation field in relation to digitized surface. Through the surface reconstruction process model is not translated into the new coordinate system, the whole reconstructed surface will be located in a coordinate system defined by TRITOP and ATOS measurement. Therefore, when determining the deviation of the surface, there is no need for any transformation of reconstructed surface. Based on deviation field of generated surface in relation to reference (digitized) mesh, figure 16, conclusion is that shown process is realized with sufficient precision.

If deviation field of generated surface in relation to reference (digitized) mesh is not convenient, some of previous phases should be repeated, figure 17. After all presented phases are performed properly, result of presented procedure is NURBS surface.

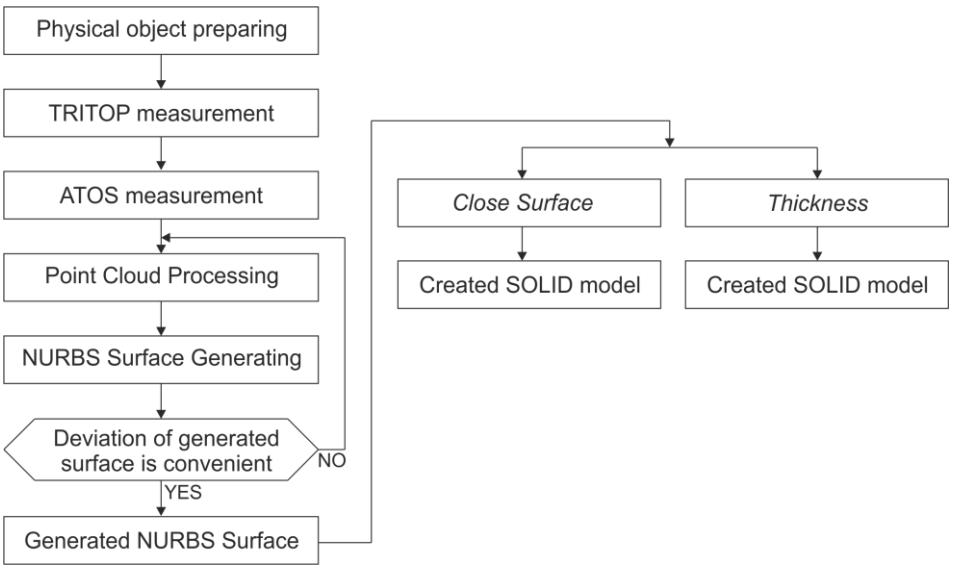

Figure 17: *Algorithm for 3D Surface Reconstruction based on Point Cloud generated by Optical Measuring Techniques*

CONCLUSIONS

The presented procedure is relatively complex, hardware- and time-consuming. It generates digitized object's surface, approximated by NURBS. This model describes surface of real physical object with high accuracy, up to 20μm. Positions of hole axis are properly transferred from TRITOP measurement and preserved during the reconstruction. The procedure for creating a closed surface model is similar. If the generated surface is open, solid model is obtained by adding thickness to surface. Otherwise, if the model's surface is closed, solid model is generated by command Close Surface.

The world's leading PLM software integrate modules for handling and processing of the point cloud, and then generating of the surface over the cloud. This fact points to the importance of this topic in the industry and R&D.

As computer digitized area is detailed description of the objects surface, also, it can be applied in 3D-Color-Digitizing, 3D Metrology, Quality Control, Shape and Dimension Control, FEA Simulation Verification, Rapid Manufacturing, 3D printing and similar purposes [4-9].

ACKNOWLEDGMENTS

This paper is created under the project of the Ministry of Science and Technological Development of the Republic of Serbia - TR12005: Software development for the explicit nonlinear dynamic analysis.

REFERENCES

[1] ATOS User Information, ATOS IIe and ATOS IIe SO (as of Rev. 01) Hardware, GOM mbH, 2008, Braunschweig, Germany,

[2] ATOS User Manual Software, ATOS v6.01, GOM mbH, 2008, Braunschweig, Germany,

[3] TRITOP User Manual Software, TRITOP v6, GOM mbH, 2008, Braunschweig, Germany,

[4] Živković M., Blagojević M., Rakić D.: The annual report on the use of received and installed capital equipment: 3D Digitization Systems ATOS IIe and TRITOP, Ministry of Science and Technological Development of the Republic of Serbia, Faculty of Mechanical Engineering in Kragujevac, Kragujevac, 2007, 2008, 2009, 2010

[5] Živković M., Blagojević M., Rakić D.: Report on the performed digitization of assemblies by 3D Digitization Systems ATOS IIe and TRITOP, Zastava Auto, Faculty of Mechanical Engineering in Kragujevac, Kragujevac, 2007.

[6] Blagojević M., Rakić D., Živković M., Bogdanović Z., Digitizing and Optical Measuring in Automotive Industry, International Congres Motor Vehicles and Motors 2008, Kragujevac, 2008.

[7] Blagojević M.: The application of optical measuring systems in modeling and simulation, Diploma work, Faculty of Mechanical Engineering in Kragujevac, Kragujevac, 2009.

[8] Blagojević M., Rakić D., Živković M., Bogdanović Z., Optical coordinate measurements of parts and assemblies in Automotive Industry, YuInfo2010, Kopaonik, 2010.

[9] Blagojević M., Rakić D., Živković M., Bogdanović Z., Dimensional stability control by optical measuring systems, IBR2010, Tara, 2010.

MVM *Editorial Board*
University of Kragujevac
Faculty of Mechanical Engineering
Sestre Janjić 6, 34000 Kragujevac, Serbia
Tel.: +381/34/335990; Tel.: 336002; Fax: + 381/34/333192
www.mvm.mfkg.kg.ac.rs